1-1-2009

The Dilemma of Disappearing Diatoms: Incorporating Diatom Dissolution Data into Paleoenvironmental Modeling and Reconstruction

David B. Ryves
Loughborough University, d.b.ryves@lboro.ac.uk

Richard W. Battarbee
University College London

Sherilyn C. Fritz
University of Nebraska - Lincoln, sfritz2@unl.edu

Published in *Quaternary Science Reviews* 28:1–2 (January 2009), pp. 120–136; doi: 10.1016/j.quascirev.2008.08.021

Submitted January 21, 2008; revised August 28, 2008; accepted August 29, 2008; published online November 30, 2008.

The Dilemma of Disappearing Diatoms: Incorporating Diatom Dissolution Data into Paleoenvironmental Modeling and Reconstruction

David B. Ryves,[1] Richard W. Battarbee,[2] and Sherilyn C. Fritz [3]

1. Department of Geography, Loughborough University, Loughborough, Leicestershire LE11 3TU, UK
2. Environmental Change Research Centre, University College London, Gower Street, London WC1E 6BT, UK
3. Department of Geosciences and School of Biological Sciences, University of Nebraska–Lincoln, Lincoln, NE 68588-0340, USA

Corresponding author — D. B. Ryves, tel 44 1509 228192, fax 44 1509 223930, email d.b.ryves@lboro.ac.uk

Abstract

Taphonomic issues pose fundamental challenges for Quaternary scientists to recover environmental signals from biological proxies and make accurate inferences of past environments. The problem of microfossil preservation, specifically diatom dissolution, remains an important, but often overlooked, source of error in both qualitative and quantitative reconstructions of key variables from fossil samples, especially those using relative abundance data. A first step to tackling this complex issue is establishing an objective method of assessing preservation (here, diatom dissolution) that can be applied by different analysts and incorporated into routine counting strategies. Here, we establish a methodology for assessment of diatom dissolution under standard light microscopy (LM) illustrated with morphological criteria for a range of major diatom valve shapes. Dissolution data can be applied to numerical models (transfer functions) from contemporary samples, and to fossil material to aid interpretation of stratigraphic profiles and taphonomic pathways of individual taxa. Using a surface sediment diatom-salinity training set from the Northern Great Plains (NGP) as an example, we explore a variety of approaches to include dissolution data in salinity inference models indirectly and directly. Results show that dissolution data can improve models, with apparent dissolution-adjusted error (RMSE) up to 15% lower than their unadjusted counterparts. Internal validation suggests improvements are more modest, with bootstrapped prediction errors (RMSEP) up to 10% lower. When tested on a short core from Devils Lake, North Dakota, which has a historical record of salinity, dissolution-adjusted models infer higher values compared to unadjusted models during peak salinity of the 1930s–1940s Dust Bowl but nonetheless significantly underestimate peak values. Site-specific factors at Devils Lake associated with effects of lake level change on taphonomy (preservation and re-working, implied by dissolution data) may override model improvements incorporating dissolution. Dissolution-adjusted salinity models are also applied to a 150-year sediment record from Spiritwood Lake, North Dakota, which suggests that this lake has a damped and lagged response to major regional climate forcing of salinity during the Dust Bowl. At this site, dissolution data also suggest different taphonomic behavior of taxa related to their seasonal patterns of growth and sedimentation. Thus, dissolution data can improve models, and aid interpretation of sedimentary profiles as records of limnological, ecological and environmental change, filtered by taphonomy.

1. Introduction

Current concern with global environmental change has highlighted the need for accurate reconstructions of past conditions to describe natural patterns of variation, and as an independent means of testing climate model hindcasts (Battarbee, 2000; Birks and Birks, 2006). Biological proxies preserved in sedimentary archives provide powerful tools for making quantitative reconstructions, often using multivariate modeling approaches. While sophisticated methods exist for such analyses, remarkably little attention has been paid to the quality of the primary data on which such models, and reconstructions, are based (Barker, 1992; Mackay *et al.*, 2005; Ryves *et al.*, 2006). Poor microfossil preservation has long been recognized as affecting all biogenic materials in certain circumstances (e.g. silica, calcite and sporopollenin; Lewin, 1961; Berger, 1968; Birks and Birks, 1980), to the extent that perfect preservation is often the exception rather than the rule. Despite much progress on understanding processes and rates of silica dissolution and biogeochemical cycling in natural systems (Conley *et al.*, 1993; Dixit *et al.*, 2001; Van Cappel-

len *et al*., 2002), little work has been carried out either to quantify the effects of preservation on inference models (Barker, 1992; Ryves *et al*., 2006) or explicitly to consider what approaches can be taken to minimize the impacts on inferences from fossil data.

Diatoms are widely used to reconstruct past aquatic environments in a range of systems (freshwater, brackish and marine; Stoermer and Smol, 1999), and are key in understanding the global biogeochemistry of silica (Tréguer *et al*., 1995). Diatom dissolution is a widespread problem in many depositional environments, particularly in saline and marine settings, but is observed in many freshwater systems too (Flower, 1993; Straub, 1993; Ryves *et al*., 2003; Bradshaw *et al*., 2005). Poor diatom preservation may be one reason why diatom-salinity models may lead to inaccurate or misleading reconstructions when applied to fossil data, especially at higher salinities (Fritz *et al*., 1993; Gasse *et al*., 1997; Reed, 1998b; Ryves *et al*., 2006). The majority of models for quantitative reconstruction using diatoms use the robust technique of weighted averaging (WA) and its derivatives (e.g. weighted averaging-partial least squares, WA-PLS; ter Braak and Juggins, 1993), whereby relative abundance (%) data are used to define species' optima, and tolerances. Other methodological approaches, such as analogue matching and maximum likelihood modeling, also rely on relative abundance data. Such approaches are susceptible to any taphonomic processes (e.g. differential transport, sedimentation and dissolution; Juggins, 1992; Cameron, 1995; Ryves *et al*., 2003) that bias the relative representation of species within, and between, the training set and fossil data. Given that it is often not possible (or desirable, from an analogue perspective; Hutson, 1977) to create models and choose fossil samples that are always well preserved, incorporating preservation data directly or indirectly into modern training sets (transfer functions) and fossil data (reconstructions) offers an explicit route to tackle preservation issues. While we focus on diatom dissolution, the approach proposed here has much wider application to a broad range of biological proxies for which taphonomic issues pose real problems for reliable interpretation of fossil data and are either discounted, or ignored.

Several possible approaches exist to the general problem of poor preservation using dissolution data (Table 1). Indirect methods include weighting species and samples according to relative resistance to dissolution, although situations in which this approach is suitable may be rare and may only result in minor improvements to model performance (Ryves, 1994). A more intuitively appealing, flexible, and potentially powerful, approach makes use of the direct (morphological) assessment of valve preservation in samples, whereby valves are classed into morphologically distinct dissolution categories, or simply classified as pristine or dissolved (Flower and Likhoshway, 1993; Ryves *et al*., 2001, 2006). Earlier work has explored qualitative and quantitative use of diatom dissolution data in contemporary and paleoenvironmental studies, to estimate the reliability of diatom-based inferences from fossil data (Barker, 1992; Ryves *et al*., 2001, 2006), but here we incorporate dissolution data directly into numerical models and reconstructions themselves (cf. Battarbee *et al*., 2005; Mackay *et al*., 2005; Austin *et al*., 2007). We also make use of dissolution data for individual taxa to help understand their taphonomic behavior and aid interpretation of stratigraphic profiles.

Dissolution indices can be used to weight species and samples directly within (or exclude them from) the training set (Table 1). Dissolution counting also can be used to create new transfer functions whereby dissolution is explicitly incorporated into the model. Each species' response along an environmental gradient can be decomposed into several constituent "dissolution taxa", each with an associated optimum and tolerance, especially where dissolution is driven partly by the parameter of interest (e.g. salinity; Fritz *et al*., 1993; Wilson *et al*., 1996; Reed, 1998a; Ryves *et al*., 2006). While species' distributions in living communities should respond to major environmental gradients (Jongman *et al*., 1995), a dissolution (taphonomic) gradient may cut across these in a fossil or sub-fossil assemblage. The replacement of one species optimum by two (or more) dissolution taxa optima may improve both model performance and quantitative inferences. Approaches that directly assess dissolution data in both training sets and fossil data are especially attractive as both datasets are treated equally (Table 1).

In some instances, valve abundances for individual taxa can be recalculated across a dataset (Battarbee *et al*., 2005; Mackay *et al*., 2005) where data on taxon-specific losses through dissolution exist (Ryves *et al*., 2001, 2003). These dissolution-corrected species' abundances can be used to derive new models and reconstructions (both qualitative and quantitative; Mackay *et al*., 2005). Dissolution-adjusted transfer functions can be compared to conventional models (e.g. Mackay *et al*., 2003, 2005) and validated both internally (by the jack-knife or bootstrap methods) and externally by comparison with an observed record of an environmental parameter, where this exists.

Here we explore the issue of a dissolution-corrected transfer function in a well known and widely applied diatom-salinity model used for paleoclimate reconstruction from lake sediments in the Northern Great Plains of America (the NGP; Fritz *et al*., 1991; Laird *et al*., 1996b, 2003, 2007). This paper develops earlier work on quantifying and predicting diatom dissolution from physical and chemical limnology, and its role as a source of error in paleosalinity reconstruction at Devils Lake, North Dakota (Ryves *et al*., 2001, 2006). This site, which has an observed record of salinity covering much of the 20th century (Fritz, 1990), provides a test case for the approaches to dissolution data discussed here. Dissolution-adjusted models and data are also applied to a ^{210}Pb-dated short core from Spiritwood Lake, North Dakota covering the last ~150 years, which can be

Table 1. Approaches to modifying training sets and fossil data according to dissolution information

Type	Dissolution information	Approach	Fossil data	Test	Reference (NGP)	Model (Table 3)
Original	None	No change	No change	Control	(Fritz, 1990), (Fritz et al., 1991, 1993); this paper	A–D
Indirect adjustment	Species' relative resistance	Downweight species and/or samples	No change	WA_{class} (CANOCO)	Ryves (1994)	–
Direct adjustment	Dissolution index for species and samples (*F*, DDI)	Downweight species and/or samples	No change	WA_{class} (CANOCO)	–	–
	Dissolution index for species and samples (*F*, DDI)	Delete samples (and/or species)	No change	WA, WA-PLS, MAT, ML	This paper	E
	Dissolution index for species and samples (*F*, DDI)	Create many new dissolution taxa	Fossil dissolution data used	WA, WA-PLS, MAT, ML	This paper	F–I
	Dissolution index for species and samples and dissolution/population relationship (*F*)	Recalculate species' abundances using dissolution index	Fossil dissolution data used	WA, WA-PLS, MAT, ML	This paper	J, K

compared to observed measurements from the lake and other nearby surface waters over the last 40–50 years.

2. Materials and methods

2.1. The Northern Great Plains datasets

Although, on an annual basis, evapotranspiration exceeds precipitation across the Northern Great Plains, topographic and groundwater conditions permit many perennial and quasi-perennial lakes to exist. Diatom communities, and surface sediment assemblages, respond strongly to the climatically controlled salinity gradient found across the wider region (Fritz *et al.*, 1993; Wilson *et al.*, 1996), and have formed the basis for diatom-salinity transfer functions for paleoclimate inference and their application at several key sites across the NGP (Fritz *et al.*, 1991; Laird *et al.*, 1996b, 2003).

The salinity models explored here are based on the models developed by Fritz (1990) and Fritz *et al.* (1991, 1993). The 55-site salinity model published by Fritz (1990) and Fritz *et al.* (1991) includes two sites (Alkaline and East Stump) with poorly preserved diatoms (and counts <100 valves) which were excluded in the 53-site salinity model of Fritz *et al.* (1993). Both these training sets (hereafter the NGP55 and NGP53 respectively) are examined here incorporating dissolution data. Additionally, an error of incorrect site attribution within earlier models has been corrected.

Many lakes within the NGP53 dataset are endorheic, from 0.1 to 28 m depth (average 5 m) and range in size from 10^{-2} km^2 to 10^2 km^2. Salinity ranges from 0.68 to 41.4 g L^{-1} total dissolved solids (TDS) in NGP53, and to 82.9 g L^{-1} TDS in NGP55 (mean 10 g L^{-1} TDS for both datasets), while pH ranges from 8.25 to 9.6 (median 8.82). Water chemistry is predominantly Na–$MgSO_4$, with carbonate precipitation at higher salinity. Full details of all NGP lakes may be found in Fritz *et al.* (1993).

2.2. Devils Lake and Spiritwood Lake

Short cores from two lakes within the NGP also were used to test the dissolution methodology. Devils Lake, North Dakota (48°05′ N, 98°56′ W) is a large (55 km^2) lake that is a terminal basin for a 10,000 km^2 watershed. Conductivity and salinity have been measured intermittently since 1899 but with a gap between 1923 and 1948, while annual water level measurements date back to 1901 (Fritz, 1990; Figure 7). A 1 m piston core was collected in January 1986 from the Creel Bay embayment in 7.5 m water. Maximum water depth in the main bay was 8.5 m in 1985 (434.8 masl). About 100 km to the south, Spiritwood Lake, North Dakota (47°05′ N, 98°35′ W) is a small, relatively deep dimictic lake (lake area 1.67 km^2, catchment area 60 km^2, maximum depth 16 m), occupying a meltwater channel, filled with glaciofluvial sediments following deglaciation (Winters, 1963). This channel is part of the Spiritwood Valley aquifer, an important component of local and regional hydrology (Huxel and Petri, 1963, 1965). In August 1991, core SW1 (82 cm long) was retrieved close to the centre of the lake using a modified piston corer in 13.4 m of water.

Both cores were extruded in the field at 1 cm intervals, and samples were stored at 4 °C prior to analysis. Dating control was achieved using ^{210}Pb (Appleby, 2001) at both sites, with a constant value subtracted for supported activity at Devils Lake (Fritz, 1990) and individual measurements of both supported and total activity at Spiritwood Lake (corroborated with measurement of ^{137}Cs and ^{241}Am; P. G. Appleby, University of Liverpool, UK; unpubl. data). A constant rate of supply model for ^{210}Pb was applied in both cases (Appleby and Oldfield, 1978) with additional dating control for Devils Lake from known regional pollen markers (Jacobson and Engstrom, 1989; Fritz, 1990).

2.3. Diatom dissolution indices

In order to include dissolution data in numerical modeling, an objective means of quantifying diatom dissolution is needed. Experimental dissolution of fresh valves and surface sediment assemblages from the NGP in a high pH medium found that groups of morphologically similar taxa (e.g. within the genera *Stephanodiscus* and *Cyclotella*) underwent similar physical patterns of corrosion as dissolution progressed (Ryves, 1994). Such patterns were also observed in deeper core material undergoing natural dissolution (e.g. *Stephanodiscus niagarae* in Figure 1), providing justification for an experimental approach as a means to quantify dissolution in natural settings. Using a combination of both light microscopy (LM) and scanning electron microscopy (SEM), dissolution patterns for each major diatom shape were defined, with 2, 3 or 4 dissolution states ("stages") identified for each taxon (stage 1 being the pristine state and higher stages indicating progressive dissolution). A description of dissolution stages for common taxa is given in Table 2 and illustrated in Figure 1 and Appendix A1 (covering 27 taxa).

During routine counting under LM, all valves (excluding girdle views) were assigned into one of the categories. Two diatom dissolution metrics can be derived from these data (F and DDI; Ryves *et al.*, 2001; Ryves *et al.*, 2006). The F (fractional) index is the proportion of pristine valves (stage 1) to all valves that can be classed (Flower and Likhoshway, 1993; Ryves *et al.*, 2001) and varies from 0 to 1, with $F = 1$ indicating all valves are perfectly preserved to $F = 0$ where all valves appear dissolved under LM. To maximize potential information from more dissolved assemblages, the "diatom dissolution index" (DDI, Ryves *et al.*, 2006) was developed, which compares the assemblage to its dissolution endpoint:

$$\mathrm{DDI} = \frac{\sum_{s=1}^{s=4} n_s(S-1)}{N(S_{\max}-1)} \quad (1)$$

where n is the number of valves in stage S, and N is the total number of valves classified (i.e. excluding girdle views). S_{max} is the highest dissolution stage that valves in the assemblage (from those present at 5% abundance or more) can reach and varies between 2 and 4. DDI also varies from 0 (perfect preservation) to 1 (all valves at highest dissolution stage for assemblage). A comparison between analysts (D. B. Ryves and R. W. Battarbee) counting 15 years apart on the US samples demonstrates that this methodology is robust for both indices (F: $r^2 = 0.89$ and DDI: $r^2 = 0.93$ for 27 NGP lakes, $p < 0.001$; Figure 2).

2.4. Diatom analysis

Original slides from the NGP surface sediment diatom training set (Fritz *et al.*, 1993) were re-examined to assess diatom dissolution of species and assemblages. Counts were made under phase-contrast LM at ×1000 magnification (mean 291 valves per lake; >300 for 45 lakes). In only two cases counts were <100 valves (Shinbone and Horseshoe). In addition, the uppermost 19 samples (count sum 150–300 valves) from the Devils Lake short core (Fritz, 1990) and 18 samples from the Spiritwood Lake short core (average count 420 valves) were counted using the dissolution methodology. Dissolution assessments of individual species important within any sample (>5% abundance) were based on at least 30-valve views of that species. Analytical effort was focused on accurately quantifying dissolution within a training set of known species composition, so as to compare the original (unadjusted) model with those incorporating dissolution data. For Alkaline and East Stump, dissolution data were obtained from original countsheets of R. W. Battarbee.

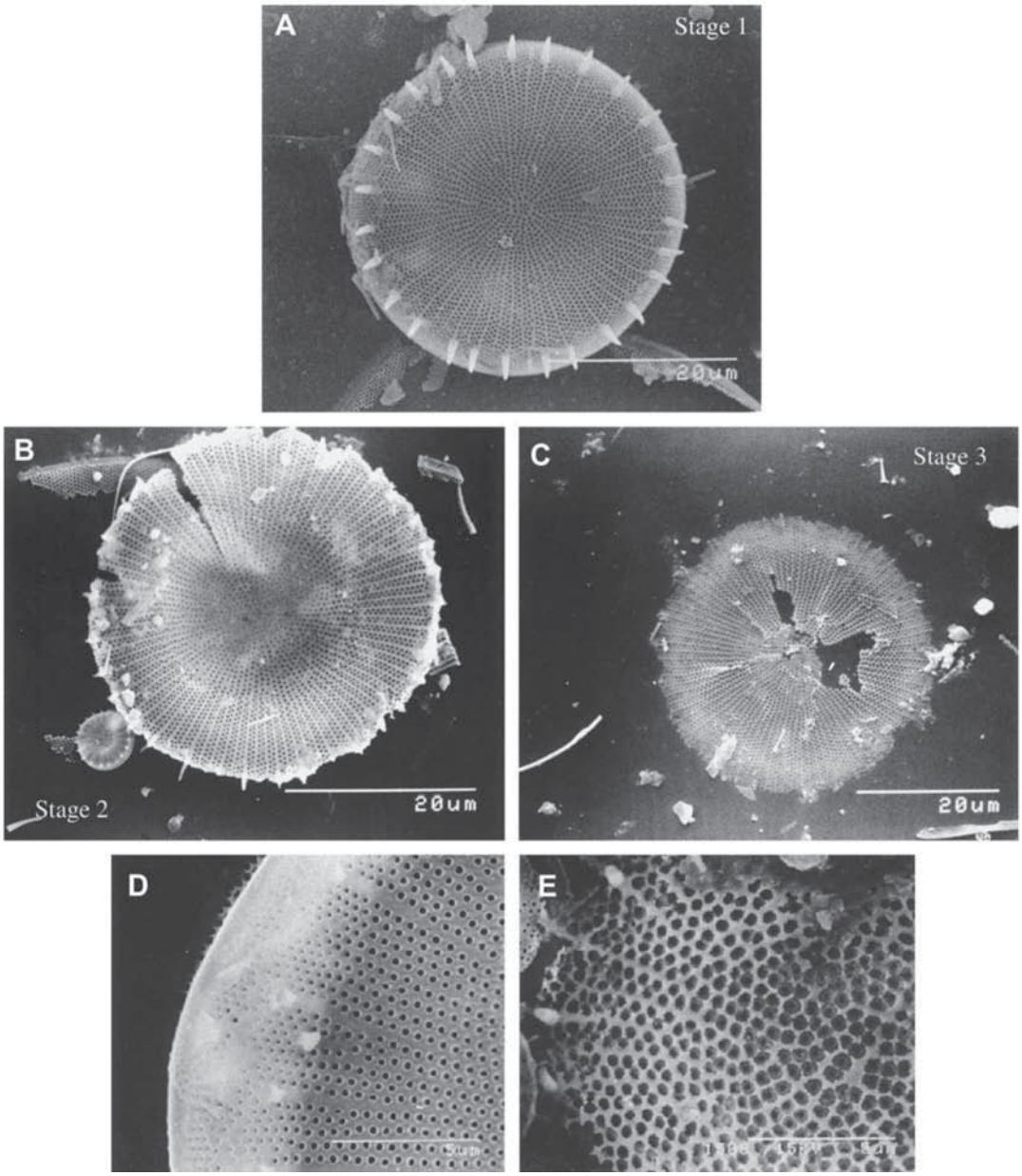

Figure 1. Dissolution stages for *Stephanodiscus niagarae* Ehrenberg (SEM micrographs of fossil material from Spiritwood Lake, ND). Stage 1 is the "pristine" state and higher stages are progressively more dissolved. A. Stage 1 showing the spines and complete valve and mantle. B. Stage 2 displays clear signs of dissolution with partial loss of the mantle and loss of finer ornamentation, e.g. spines. Note also the valve starting to fracture along striae with areolae, starting to enlarge under dissolution. C. Stage 3 is the highest stage recognized for this taxon. All spines are gone and the mantle is removed. Parts of the valve face may be missing. D. Details of a valve in stage 1 (A) – areolae are not noticeably dissolved. E. Detail of stage 3 – areolae are enlarged and starting to coalesce as dissolution progresses, creating lines of structural weakness along the valve.

Diatom identification followed standard texts (Patrick and Reimer, 1966, 1975; Krammer and Lange-Bertalot, 1986, 1988, 1991a, 1991b), more specialist publications dealing with specific saline lake taxa found in the NGP (e.g. Battarbee *et al.*, 1984; Carvalho *et al.*, 1995) and informal saline diatom taxonomy workshop protocols. Initially, raphid and araphid valves from heterovalvar taxa (e.g. *Achnanthes* spp., *Cocconeis* spp. and *Rhoicosphenia curvata*) were enumerated separately during dissolution counting, as they may show different dissolution behavior (Ryves *et al.*, 2001). *Chaetoceros* cysts (thought to be *Chaetoceros elmorei* or *C. muelleri*; Fritz *et al.*, 1993) were classed as stage 2 unless associated with the weakly silicified enclosing cell (considered stage 1), but no further dissolution stages could be reliably identified for this taxon.

2.5. Numerical analyses

Dissolution data obtained directly during routine counting of training sets and cores can be used to create new inference models in several ways (Table 1). One approach is to consider the distribution of each dissolution stage of every taxon as a pseudospecies in its own right, which appears logical as dissolution is correlated to salinity within the NGP (Ryves *et al.*, 2006). For this method, the original percentage abundance of each species in every sample (as found by Fritz *et al.*, 1993) was split amongst its constituent "dissolution taxa" (undissolved or corroded under the *F* index, and with up to four stages using the DDI methodology). This was calculated using the relative proportion of valves in each dissolution stage found under the recount for

Table 2. Dissolution stages for some major morphological groups. See Appendix A1 for illustrations.

Stage 1 is the pristine condition in all cases

Amphora
Stage 2. Striae at distal raphe ends dissolve and coalesce. Areolae enlarged throughout valve
Stage 3. Valve dissolves from distal raphe ends, particularly along dorsal margin, which may quickly disappear
Stage 4. Central hyaline area of thicker silica remains; raphe, if present, vestigial. No striae remain

Anomoeoneis
Stage 2. Areolae/ocelli enlarged; valve walls noticeably thinner

Stage 3. Valve dissolves from margins to raphe, and from apices to centre. Valve may split along raphe canal. Identification is by central area

Campylodiscus
Stage 2. Inter-costal area corrodes at margin; central area persists

Stage 3. Central area tends to dissolve before the marginal ribs, which are progressively exposed. Raphe and ribs remain, usually at expense of inter-costal and central areas

Cocconeis – (araphid valve)
Stage 2 Areolae enlarged; marginal rim dissolved. Valve may split along apical axis

Cocconeis + (raphid valve).
Stage 2. Areolae enlarged; raphe often resists dissolution relative to the surrounding valve face. Valve may split along raphe

Cyclotella
Stage 2. Inter-costal areas dissolve but marginal rim remains
Stage 3. Costae remain but marginal rim dissolved
Stage 4. Costae dissolved or vestigial; central area (with processes enlarged) may survive as a featureless disc

Cymbella
Stage 2. Distal valve ends dissolve from both margins towards raphe
Stage 3. Raphe and central area remain; striae dissolved but silica ribs separating striae remain. Both margins dissolved

Naviculoid pennate – e.g. *Navicula oblonga*, *Mastogloia* spp.
Stage 2. Chambers of striae coalesce, especially at distal raphe ends. Valve outline maintained. Margins remain
Stage 3. Valve dissolves from distal apices towards central area. Valve margins distinguishable towards center
Stage 4. Central area only remains, with vestigial raphe canal

Nitzschia
Stage 2. Areolae coalesce; striae dissolve; often raphe (and keel punctae) only remain

Stephanodiscus
Stage 2. Areolae enlarged and may coalesce; margins remain. Spines often corroded, irregularly preserved
Stage 3. Valve dissolves from margin towards central area; margin dissolved. Spines disappear.

Surirella
Stage 2. Inter-costal area corrodes at margin; central area and raphe persists
Stage 3. Marginal raphe and central area remain; inter-costal area dissolved

Synedra
Stage 2. Striae chambers coalesce and dissolve at valve margins; valve apices distinct.
Stage 3. Valve dissolves towards central area from apices

that species in that sample. For any sample where taxa were not recorded during the recount (i.e. rare taxa not encountered due to smaller counts or different transects viewed under LM), the average dissolution index for the sample was used. The original distribution of Fritz *et al.* (1993) across the dataset for all species was thus maintained and provides a direct comparison with the unadjusted NGP models.

A second method involved using the *F* values for each species in each sample as an indicator of taxon-specific valve loss within that sample, using the empirical relationship observed from dissolution experiments for mixed assemblages (Ryves *et al.*, 2001). A dissolution correction factor can be applied to each occurrence (y_{ij}) of species *j* in any sample *i*, and then new abundances ($F[y_{ij}]$) calculated for each species in every sample as follows:

$$F\left[y_{ij}\right] = \frac{y_{ij}F^*_{ij}}{\sum_{j=1}^{j=j} y_{ij}F^*_{ij}} \quad (2)$$

The dissolution correction factor, F^*_{ij}, for any species' occurrence is derived from re-arranging the relationship between *F* and valve loss in Ryves *et al.* (2001):

$$F^*_{ij} = 10^{0.979-1.075F_{ij}} \quad (3)$$

where F_{ij} is the *F* index for species *j* in sample *i*. Values of range from 9.5 when $F = 0$, and are capped at 1 where preservation is excellent ($F \geq 0.91$). To avoid introducing excessive noise from species found at low abundance, the original dataset was screened and taxa occurring at <1% maximum abundance deleted. Taxa that were not recorded in this reduced dataset during the dissolution recount were assigned the assemblage *F* value for that sample. These models can be directly compared to unadjusted NGP models screened with a 1% cut-off (e.g. Fritz *et al.*, 1993).

Transfer function development was carried out within the C2 program (version 1.4.3; Juggins, 2003). Diatom assemblage data were analyzed as percentages but were otherwise untransformed. Salinity (expressed as g L^{-1} TDS) was log transformed to approximate normality and reduce the influence of large values. C2 includes all weighted averaging (WA) variants (WA with both classical and inverse deshrinking, and with tolerance downweighting of taxa), as well as WA-PLS, analogue matching (MAT) and maximum likelihood modeling (ML). Inverse deshrinking tends to improve overall model performance (lower errors), but may lead to less accuracy at extreme ends of the environmental gradient. Models were internally validated using the bootstrap method in C2 (1000 cycles; Birks *et al.*, 1990). Apparent and predicted root-mean square errors (RMSE and RMSEP) values are reported as $\log_{10}$ TDS. Salinity optima for species (and dissolution pseudospecies) were derived using WA.

User-defined weighting for individual samples and species within C2 is only available by deletion (zero weight; Table 1) but can be implemented within CANOCO to derive a simple WA transfer function with classical deshrinking (ter Braak and Šmilauer, 2002), although there is no straightforward method of assessing predictive error. Given these restrictions, weighting of samples and species using either directly observed dissolution data, or indirectly according to relative resistance to dissolution was not tested in the current study. Previous work using variable weighting based on species' relative resistance to dissolution derived from experiments has suggested that generally only minor improvements can be expected (Ryves, 1994).

Model validation against the Devils Lake salinity record was based on a short core covering the period of historical salinity measurements (Fritz, 1990). Salinity (or conductivity) has been measured sporadically at Spiritwood Lake since the mid-1970s (M. Sauer, North Dakota Department of Health, pers. comm.), with isolated values from 1965 to 1972 (G. Van Eeckhout, North Dakota Game and Fish Department, pers. comm., Tarapchak, 1973; values converted to salinity). Although no measured data exist for earlier periods, there is some anecdotal evidence for lake level change from written accounts over the last century (Johnson, 1950). There are also measurements of conductivity since the 1950s for the James River (46°53′23″ N, 98°40′54″ W) and Jamestown Reservoir (46°55′50″ N, 98°42′23″ W) obtained from the

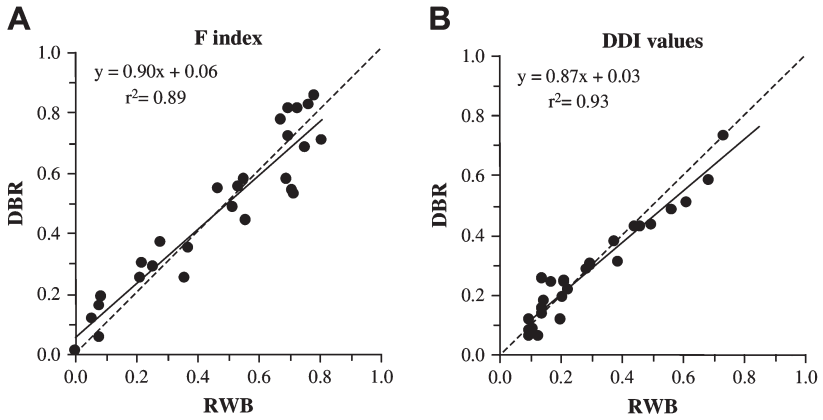

Figure 2. Correlation between (A) *F* index and (B) DDI values for 27 NGP lakes independently counted by D. B. Ryves (DBR) and R. W. Battarbee (RWB). Dotted line is the 1:1 correlation.

USGS National Water Interface System (http://nwis.waterdata.usgs.gov/nd/nwis/), both within the same major catchment as Spiritwood Lake and about 15–18 km to the south-west. Goodness-of-fit of reconstructions also were estimated statistically by comparing fossil and training set squared residual distances from a single-variable CCA salinity axis (Birks *et al.*, 1990). If fossil samples lie in the upper 10% or 5% of the distribution of such distances in the surface sediments (log transformed for normality), they are deemed to have a "poor" or "very poor" fit respectively to the reconstructed variable (Birks *et al.*, 1990; Laird *et al.*, 1996a).

3. Results

3.1. Dissolution taxonomy and methodology

There is excellent agreement between taxonomists for both *F* and DDI with the slopes for both indices indistinguishable from 1 (Figure 2). Given the time interval separating these counts, this suggests that objective criteria for assessing dissolution exist and are robust. Four dissolution stages were recognized for common *Cyclotella*, larger *Amphora* and Naviculoid taxa; three for many other pennates (e.g. *Anomoeoneis*, *Gomphonema*, and other smaller Naviculoid taxa), centrics (*Stephanodiscus*) and Surirellaceae; and two for fine and/or small taxa such as many *Nitzschia*, *Cocconeis* and *Achnanthes* species (Table 2, Figure 2, Appendix A1). Descriptions for each dissolution stage (Table 2) are based on their appearance under LM at ×1000 so that the method can be used during routine counting. SEM imagery, however, shows that substantial dissolution can occur before valves appear dissolved under LM (Appendix A1), with areolae becoming enlarged (cf. Figure 1E) and silica surfaces developing a "spongy" appearance in valves otherwise classed as pristine under LM.

3.2. Dissolution pseudospecies within the NGP

As diatom dissolution is correlated with salinity, salinity optima calculated for successive dissolution stages of an individual species should progressively increase and is the logic by which dissolution data may improve diatom-salinity models and inferences. Figure 3 shows the WA salinity optima for all dissolution stages for the 39 species in NGP53 that have a maximum abundance of at least 10% and occur in 5 lakes or more, with 4 species split into raphid and araphid forms (though all taxa above specified cut-off values are included in the models; Table 3). For 31 taxa (72%), less dissolved valves have lower salinity optima than more dissolved, and these often plot in numeric order where 3 or 4 stages are recognized. Dissolution salinity optima can span the species optimum by 0.5 log-salinity units or more, equivalent to a factor of 3. For example, NA054A (*Navicula veneta*; Figure 3) has a salinity optimum of 4.94 g L^{-1} TDS, representing the weighted average of its three component dissolution stages, with optima of 2.74 (stage 1 = undissolved), 4.95 (stage 2) and 14.71 (stage 3) g L^{-1} TDS respectively; *Cyclotella quillensis* (CY017A; optimum 12.53 g L^{-1} TDS) has 4 dissolution stages (spanning 8.17–14.68 g L^{-1}).

Figure 3 suggests there are only minor differences in the salinity range of raphid and araphid valves, in contrast to results from dissolution experiments which found sometimes large differences in robustness between these valve types (Ryves *et al.*, 2001). Such differences may be obscured by other taphonomic effects during transport and sedimentation of these periphytic taxa from their littoral habitats to offshore, deeper water sediments. In the light of this, heterovalvar species were not separated into raphid and araphid taxa within NGP dataset for subsequent transfer function development.

Many of these dissolution taxa exhibit a unimodal response to salinity as does the species from which they derive, an assumption of WA methods. Figure 4 and Figure 5 show the distribution with respect to salinity of *C. quillensis* (for both NGP53 and NGP55) and *Navicula cincta* for all observations and separated according to dissolution stage (4 stages for *C. quillensis* and 3 for *N. cincta*). The estimated WA salinity optima and the modeled response under logistic regression (predicted unimodal fit) for NGP53 are in close agreement and suggest true unimodal response for these dissolution taxa, even for pseudospecies that do not show large increases in salinity optima for successive dissolution stages (e.g. *N. cincta*, Figure 5). These results suggest that the distribution of some taxa, and so their "aggregate" WA optima, are strongly influenced by dissolution. In particular, the species optimum for *C. quillensis* is largely defined by badly preserved samples as most valves in the NGP are dissolved (stage 1 optimum of 8.17 g L^{-1} TDS; Figure 4). Including East Stump (77% *C. quillensis*, all stage 3 or 4) in the training set increases the species salinity optimum from 12.53 to 16.22 g L^{-1} TDS, through its effect on optima for stages 3 and 4 while leaving stages 1 and 2 optima unchanged (Figure 4). This clearly has implications for ecological inferences made from surface sediment training sets that are affected by such taphonomic effects, where the surface sedimentary abundances may not be an accurate reflection of the living community.

3.3. Dissolution-adjusted salinity models

Table 3 summarizes the results of modeling experiments incorporating dissolution information (Table 1) on the NGP training sets using a variety of indirect and direct approaches (models E–K) compared to unadjusted models (A–D). For dissolu-

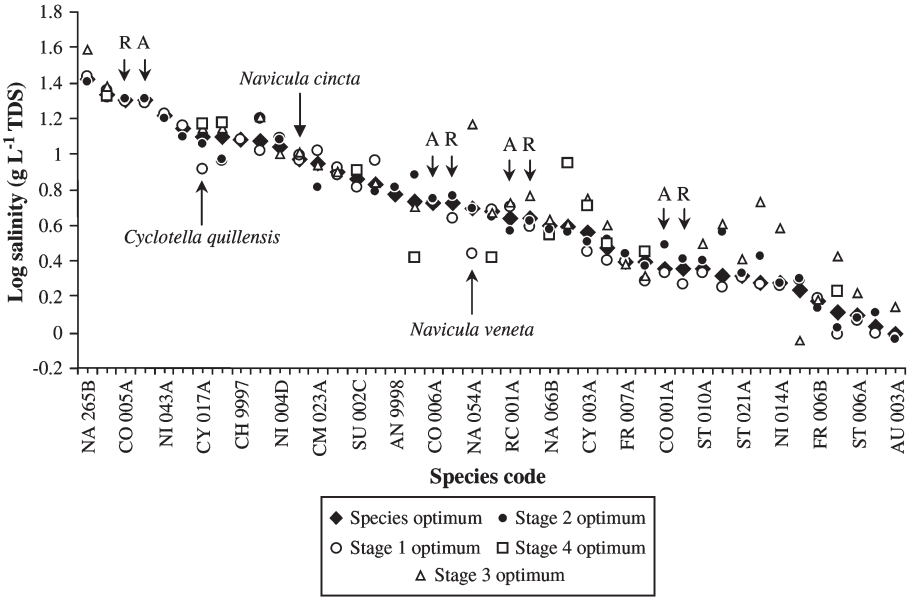

Figure 3. Salinity optima (weighted average, log TDS, g L^{-1}) of the most abundant taxa in the NGP dataset (ordered according to species optimum of all valves without reference to dissolution state). For each species, salinity optima for each dissolution stage (1–4, depending on species) are also plotted (dissolution pseudospecies). A = araphid valve; R = raphid valve. Species mentioned in the text are indicated.

tion-adjusted models (Table 3, E–K), WA methods outperformed WA-PLS, MAT and ML methods in all cases. For each training set, the "best" apparent and predicted models are shown (as judged by lowest RMSE and RMSEP respectively). In all cases, the best apparent models (lowest RMSE) were produced under WA with tolerance downweighting and inverse deshrinking ($WAtol_{inv}$), while lowest predicted errors (minimizing RMSEP) were found using simple WA models (but always under inverse deshrinking for models ignoring dissolution, and classical deshrinking for those incorporating dissolution information).

The unadjusted NGP models (Table 3, A–D), with all taxa and a cut-off of 1%, appear robust with low RMSE (around 0.17 log-salinity units, LSU). These errors are likely underestimated, however, as the bootstrapping analysis shows, with RMSEP of around 0.3 LSU. Models display apparent systematic underestimation at higher salinity, which correlates to some extent with dissolution state of the training set sample (Figure 6A), although when residuals are plotted against predicted values (Racca and Prairie, 2004) this trend disappears. Models tend to improve as the number of taxa increases, in agreement with other studies (Wilson *et al.*, 1996; Birks, 1998). Within its salinity range, all NGP salinity transfer functions compare favorably with a 219-lake training set from British Columbia (Wilson *et al.*, 1996; salinity range 0.02–620 g L^{-1} TDS, no. of taxa 204, r^2 = 0.87, $RMSE_{boot}$ = 0.371 LSU), and others (e.g. Gasse *et al.*, 1995; Reed, 1998a; Davies *et al.*, 2002; Yang *et al.*, 2003).

All transfer functions making use of dissolution data produce models that appear to perform better, though these improvements are minor when validated under bootstrapping compared to the unadjusted models (Table 3, E–K). Under model E (NGP53), deleting four samples that are badly preserved (F < 0.15; Bitter (South Dakota), George, Hazelden and Rabbit) removes only one lake with a residual >0.3 LSU (Hazelden; Figure 6). Samples from Mission Bay, Boucher, Porter and Eckelson all have residuals >0.4 LSU but are better preserved.

By definition models built using dissolution pseudospecies contain many more taxa than the unadjusted training set, with 365 taxa where species are separated into pristine and dissolved categories (Table 3, F and G), and 536 taxa where all dissolution stages are considered (Table 3, H and I). These two

Table 3. NGP diatom-salinity model results under various dissolution-dependent strategies

Code	Dataset	No. of taxa	No. of lakes	Data screening	Best apparent			Best predicted		
		j	*i*	**Value**	**Model**	r^2	**RMSE**	**Model**	r^2_{boot}	**RMSEP**
Unadjusted models										
A	Original (NGP53)	258	53	–	$WAtol_{inv}$	0.91	0.158	WA_{inv}	0.72	0.291
B	Original (NGP53)	148	53	1%	$WAtol_{inv}$	0.91	0.158	WA_{inv}	0.74	0.284
C	Original (NGP55)	258	55	–	$WAtol_{inv}$	0.89	0.178	WA_{inv}	0.70	0.309
D	Original (NGP55)	149	55	1%	$WAtol_{inv}$	0.89	0.178	WA_{inv}	0.72	0.302
Dissolution-adjusted models										
E	Original – deleted sites	255	49	F < 0.15	$WAtol_{inv}$	0.91	0.153	WA_{class}	0.71	0.294
F	Dissolution – binary	365	53	–	$WAtol_{inv}$	0.93	0.141	WA_{class}	0.73	0.286
G	Dissolution – binary	365	55	–	$WAtol_{inv}$	0.91	0.159	WA_{class}	0.71	0.305
H	Dissolution – all stages	536	53	–	$WAtol_{inv}$	0.93	0.135	WA_{class}	0.73	0.286
I	Dissolution – all stages	536	55	–	$WAtol_{inv}$	0.92	0.149	WA_{class}	0.72	0.302
J	*F* adjusted	148	53	1%	$WAtol_{inv}$	0.90	0.162	WA_{class}	0.75	0.276
K	*F* adjusted	148	52	1%	$WAtol_{inv}$	0.92	0.145	WA_{class}	0.77	0.261

Predictions are based on 1000 bootstrap cycles. Data screening (where applied) indicates the cut-off value below which species (as relative abundance, %) or samples (F scores) were deleted. RMSE and RMSEP values are log-salinity units (g L^{-1} TDS).

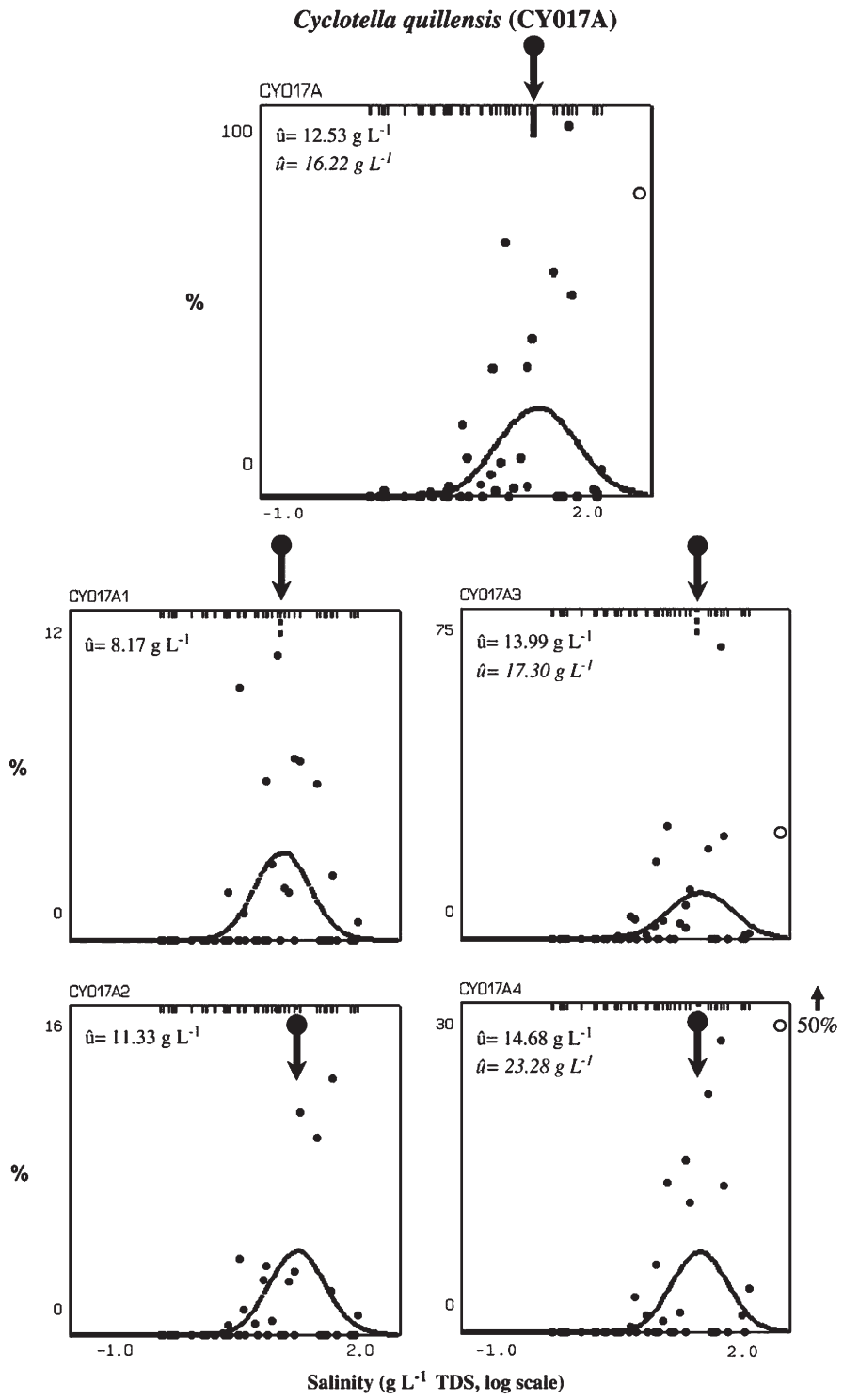

Figure 4. Species abundance (%) across the NGP dataset for *Cyclotella quillensis* Bailey (CY017A; see Figure 3). Upper plot: Species distribution for all valves. Lower plots: Distributions for the 4 dissolution pseudospecies recognized for this species (CY017A1 = stage 1, CY017A2 = stage 2, CY017A3 = stage 3, CY017A4 = stage 4). **û** = weighted average (WA) optimum, g L^{-1} TDS, indicated by the down arrow in each plot. Adding East Stump to the training set (empty circles) alters the WA optimum for stages 3 and 4, and hence optimum for all occurrences (shown in italics). Solid line is modeled response under logistic regression (predicted unimodal fit).

approaches produce models with the lowest apparent RMSE values generated (0.14 LSU for 53 sites), a marked improvement on unadjusted models (15% lower). RMSEP values are not better, however (0.3 LSU). Recalculating species' abundances using the *F* index (Table 3, J) produced models with similar RMSE to unadjusted models, and marginally lower RMSEP, though still 0.28 LSU. Examination of the residuals of model J against predicted salinity of the training set lakes (Racca and Prairie, 2004) suggested that Eckelson Lake was an outlier (0.55 LSU; cf. Figure 6B), which is not the case with unadjusted NGP53 models (Figure 6A). Deleting this site improved the model further (model K; Figure 6B, Table 3), with both RMSE and RMSEP 10% lower than any of the unadjusted models, and appears to reduce bias at high salinity (Figure 6B).

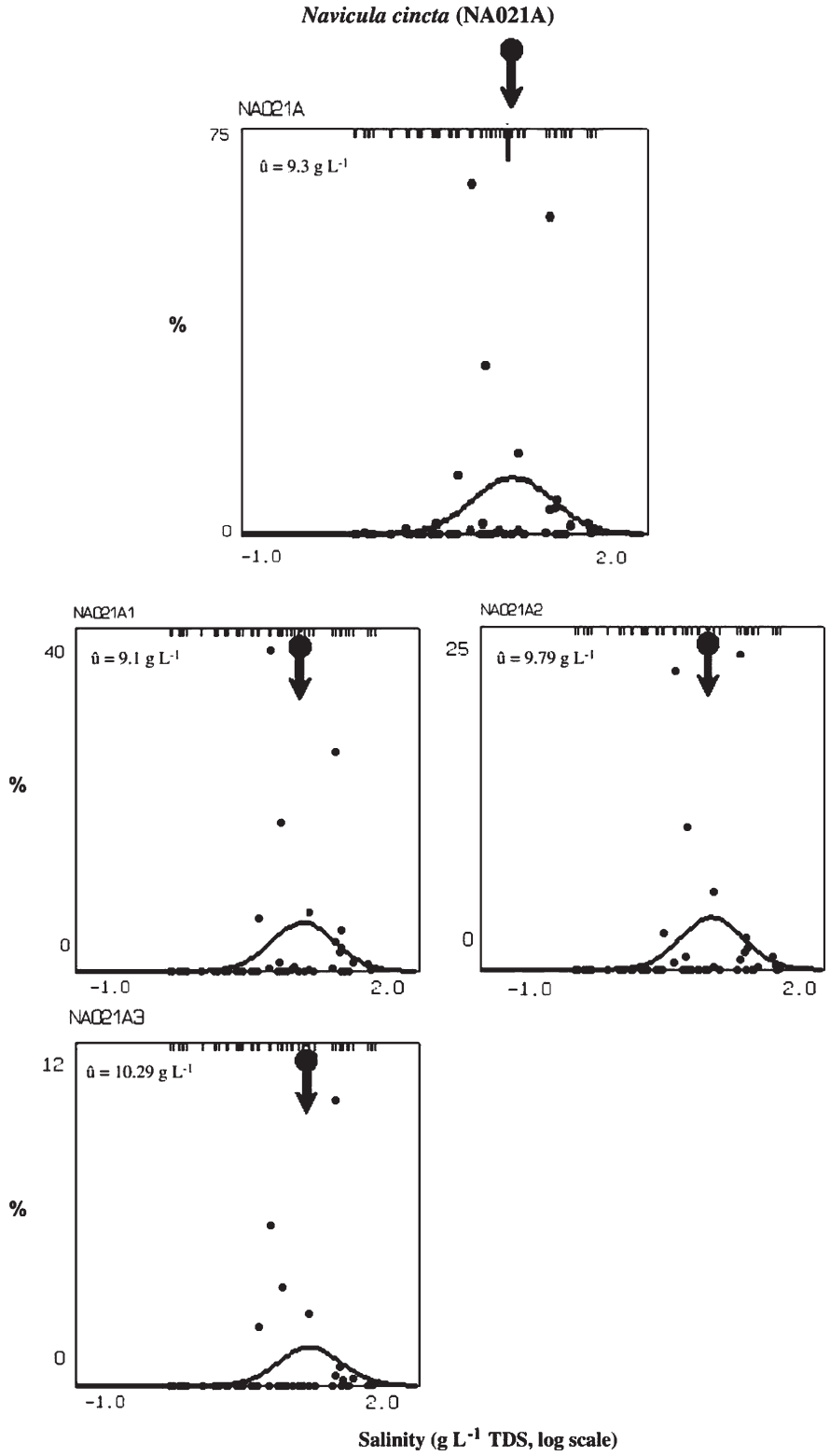

Figure 5. Species abundance (%) across the NGP dataset for *Navicula cincta* (Ehrenberg) Ralfs (NA021A; see Figure 3). Upper plot: Species distribution for all valves. Lower plots: Distributions for the 3 dissolution pseudospecies recognized for this species (NA021A1 = stage 1, NA021A2 = stage 2, NA021A3 = stage 3). **û** = weighted average (WA) optimum, g L^{-1} TDS, indicated by the down arrow in each plot. Solid line is modeled response under logistic regression (predicted unimodal fit).

3.4. Application of salinity models at Devils Lake and Spiritwood Lake

Summary diatom diagrams are shown for Devils Lake (Figure 7, adapted from Fritz, 1990) and Spiritwood Lake (Figure 8) including all taxa found at >5% in any sample. The proportion of pristine and dissolved valves for each of the taxa found in each sample are indicated, together with sample *F* index, observed lake level and salinity (Devils Lake) and sedimentation rate data (Spiritwood Lake).

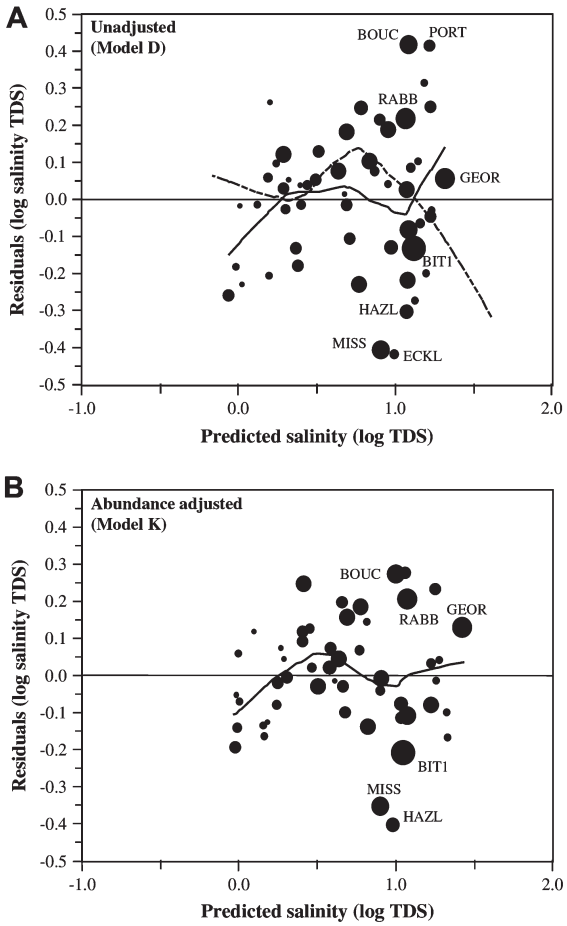

Figure 6. A. Plot of residuals (log TDS, g L^{-1}) against predicted salinity for model D (Table 3) sized according to dissolution index (DDI). Sites mentioned in the text are labelled. Solid line is LOESS smoother added through data. Dotted line is LOESS smoother when residuals are plotted against observed salinity. B. Plot of residuals (log TDS, g L^{-1}) against predicted salinity for model K (Table 3) with the outlier Eckelson Lake removed. Points are sized according to dissolution index (DDI). Sites mentioned in the text are labelled. LOESS smoother added through data.

3.4.1. Devils Lake diatom stratigraphy

The recent diatom record at Devils Lake is discussed in detail in Fritz (1990) and only a brief summary is given here (Figure 7). Over the last 100 years, Devils Lake shows dramatic shifts from an assemblage dominated by freshwater planktonic *Stephanodiscus* taxa (*Stephanodiscus minutulus* and *S. niagarae*) to one dominated by saline planktonic species, especially *C. quillensis* and *Chaetoceros* cysts, in keeping with the observed (and inverse) trends in lake level and salinity. Diatom dissolution is significant (*F* 0.4; Ryves *et al.*, 2006) for all samples before 1960, even when water levels were high in the early 20th century.

3.4.2. Spiritwood Lake diatom stratigraphy

The diatom record at Spiritwood Lake (Figure 8) is dominated by planktonic taxa throughout, especially *S. minutulus* and *S. niagarae*, which tend to co-vary inversely (and may reflect Si:P availability and water column turbulence). The flora is indicative of freshwater (<0.5 g L^{-1} TDS) to subsaline (0.5–3 g L^{-1} TDS) conditions throughout much of the recent past. A period of elevated salinity is suggested in the 1940s and 1950s, when *Cyclotella meneghiniana* (and the appearance of *C. quillensis*) and *C. elmorei/muelleri* cysts make up over 30% of the assemblage. Throughout the 1980s, the epiphytic *Cocconeis placentula* becomes important, declining in the upper samples with the rise of the planktonic freshwater *Fragilaria capucina* var. *mesolepta*, in concert with lake management practices to reduce total phosphorus (TP) concentrations. The surface sediment is dominated (80%) by very well preserved *F. capucina*, likely reflecting a summer bloom when the lake was cored (August 1991).

The *F* index fluctuates between 0.2 and 0.6 throughout the record before 1970, when there is a transition to higher values indicating better preservation (reaching 0.9 in the surface sample). Sediment accumulation rates reflect the long term rise in agricultural intensification throughout the region since European immigration in the 19th century, falling in the 1950s and 1960s, but increasing to the present.

3.4.3. Salinity inference at Devils Lake and Spiritwood Lake

Both original models (i.e. ignoring dissolution) and dissolution-adjusted models were applied to the Devils Lake and Spiritwood Lake short cores and compared with measured salinity at both sites (Figure 9). Results are shown for comparable 55 and 53 lake datasets with lowest RMSEP (models A, C, F and G in Table 3). At each site, the general patterns of salinity inference are similar, and at Devils Lake (Figure 9A), all reconstructions are significantly correlated with observed salinity ($p < 0.01$, $n = 15$). Sample-specific errors are substantially lower than predicted (RMSEP), in all cases being 0.1 LSU (20% of the back-transformed value), and hence profiles of inferred salinity show significant differences both within and between models at each site.

The effect of deleting Alkaline and especially East Stump (the latter dominated by dissolved *C. quillensis*) is clear at Devils Lake as DI-salinity values are significantly lower under the NGP53 models. At salinity above 5 g L^{-1} TDS at Devils Lake, dissolution models tend to infer higher values relative to their unadjusted counterparts, particularly in samples before 1950, where most valves are dissolved, although highest salinity values in the 1930s–1940s are likely underestimated under all models (but here there are no observed salinity data for comparison). Conversely, dissolution models appear to overestimate salinity in the late 19th century compared to unadjusted models. DI-salinity tends to be inversely related to sample dissolution index, and this relationship is emphasized by dissolution models.

Inferred salinity at Spiritwood Lake (Figure 9B) over the last 150 years is relatively low compared to Devils Lake, with values between 1 and 3 g L^{-1} TDS (depending on model) for much of this time, except during a period of elevated salinity in the 1940s–1950s. At Spiritwood Lake, salinity inference under the 55-site models tends to be higher than the 53-site models in all cases, again except for low values from the mid-1970s, where all models infer very similar values. Dissolution models differ little from unadjusted models at this site, except during the 1940s–1950s. The NGP55 dissolution model (G, Table 3) infers the highest salinity of all models in the mid-1950s (almost 5 g L^{-1} TDS), suggesting that salinity was above the saline threshold (3 g L^{-1} TDS) from the 1940s, in contrast to other models (including the NGP53 dissolution model). All DI-inferred values agree well with salinity measurements at the lake from the mid-1970s when salinity was low, but observed salinity in 1970 and especially 1965 agree better with the dissolution models. Although few measurements of lake salinity exist, summer conductivity data (i.e. post ice-out and spring melt) for the James River (June–September, averaged over 3–5 years from 1949/1950) and Jamestown Reservoir (yearly May–October averages, from 1959) show good agreement (within dating errors) with inferred (summer) salinity patterns at Spiritwood Lake, and provide some confidence that models have captured the general salinity trends at this site. As at Devils Lake, the *F* index varies inversely to DI-salinity, even at these low inferred values.

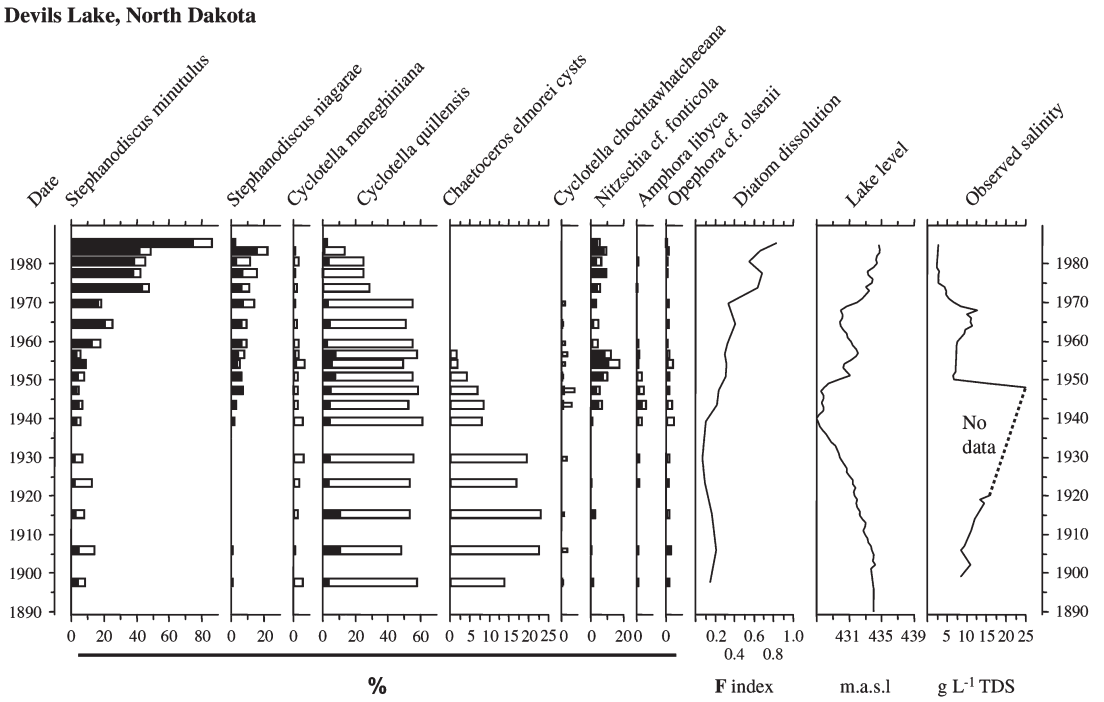

Figure 7. Summary diatom diagram (%) for Devils Lake short core, North Dakota (after Fritz, 1990). Hollow bars indicate proportion of valves dissolved for each species. Thin bars are ×5 exaggeration. Also plotted are sample *F* index, measured lake level and observed salinity.

4. Discussion

4.1. Developing a dissolution taxonomy

Repeatable dissolution patterns exist for many valve shapes observable under LM across different aquatic systems (Flower, 1993; Barker *et al.*, 1994; Mackay *et al.*, 1998), and the strong agreement between different taxonomists (using independently derived dissolution schemes) suggests that these can be objectively defined. While previous research has used the dissolution state of one, two or three common taxa to categorize sample preservation (e.g. Barker, 1992; Flower and Likhoshway, 1993; Mackay *et al.*, 1998; Warnock *et al.*, 2007), basing an assessment upon all valve views counted allows samples to be compared across very different ecological and limnological (or oceanographic) conditions and reduces possible errors from low abundance or re-working that may affect any single taxon. Evaluating dissolution under LM may not be as accurate or detailed as

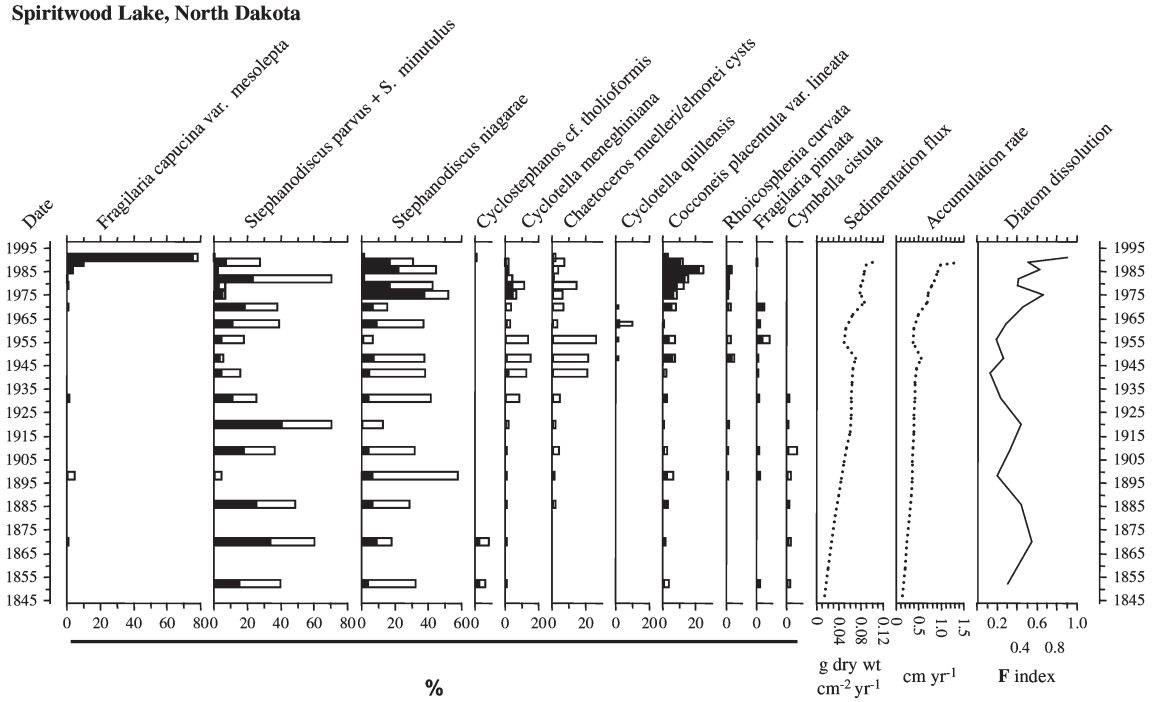

Figure 8. Summary diatom diagram (%) for Spiritwood Lake short core, North Dakota. Hollow bars indicate proportion of valves dissolved for each species. Thin bars are ×5 exaggeration. Also plotted are sedimentation rate (flux and accumulation) and sample *F* index.

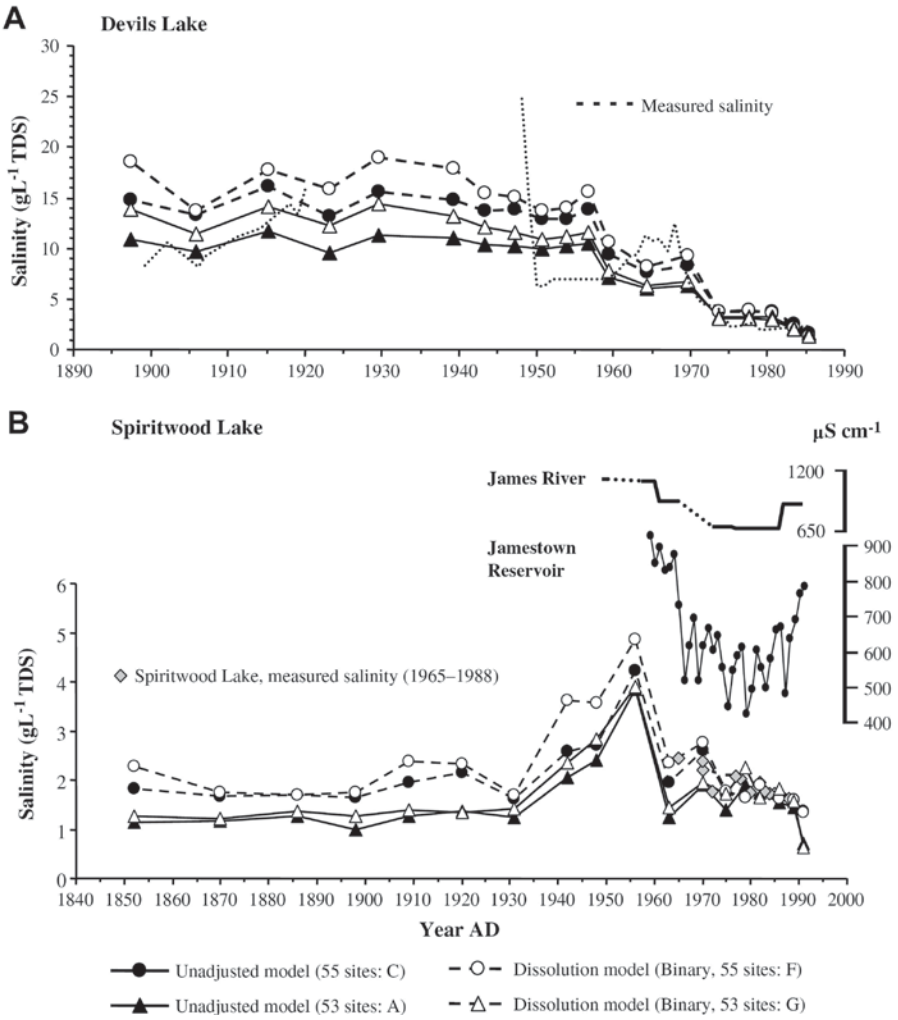

Figure 9. Diatom-inferred salinity for short cores from (A) Devils Lake and (B) Spiritwood Lake, using comparable 53- and 55-site NGP models both ignoring (models A and C, Table 3) and incorporating dissolution data (models F and G, Table 3). At Devils Lake, measured salinity values are shown by the dotted line. For Spiritwood Lake, shaded diamonds are measured mean summer salinity values (1965, 1970, 1972: data supplied by G. R. Van Eeckhout; 1970: from Tarapchak, 1973, conductivity converted to salinity; 1977–1988: values from M. Sauer, pers. comm.). Also plotted are summer conductivity values for nearby surface waters (the James River and Jamestown Reservoir) from 1950, collated from data from the USGS National Water Interface System.

under SEM (e.g. Warnock *et al.*, 2007) but can be easily incorporated into routine counting strategies, without the need for additional sample preparation and analysis.

Dissolution stages for taxa not included here can be easily established by LM examination of material across the full range of dissolution state (ideally obtained from dissolution experiments, where other factors, such as breakage, can be controlled). Examination under SEM can support this and demonstrates that extensive valve corrosion occurs before effects are noticeable under LM. This may help explain the exponential decline of valve number with increasing dissolution (as recorded by *F* or DDI; Ryves *et al.*, 2001), as weakened valves may easily break into uncountable fragments leaving a much reduced residual assemblage identifiable during progressive dissolution. Previous work has noted the strong relationship between dissolution and fragmentation in both surface sediments (Ryves *et al.*, 2006) and core studies in both freshwaters (Straub, 1993) and marine sediments (Warnock *et al.*, 2007).

Many of the key taxa in the NGP model are also found in other diatom-salinity training sets (e.g. Wilson *et al.*, 1996; Reed, 1998a; Yang *et al.*, 2003), and the dissolution sequences identified and illustrated (Table 2, Appendix A1) should be applicable and adaptable elsewhere to a wide range of taxa of similar morphology. Under certain pore water conditions, dissolved silica may re-precipitate onto frustules as amorphous silica or more complex silica minerals (e.g. zeolites), hampering identification along a dissolution sequence, and under extreme circumstances rendering diatom identification impossible (Barker *et al.*, 1994; Gasse *et al.*, 1997).

4.2. Incorporating dissolution data into models

Dissolution experiments allow taxa to be ranked according to their susceptibility to dissolution, and offer an indirect means of incorporating dissolution data into models by downweighting resistant species (and/or samples, if weighted by the rank of constituent species; Ryves, 1994). Although many studies have used the presence or proportion of robust and/or susceptible taxa as indicative of dissolution (e.g. Johnson, 1974; Shemesh *et al.*, 1989; Pichon *et al.*, 1992) weighting species and samples according to dissolution resistance is an ad hoc approach to the more fundamental problem of actual sample and species preservation within training sets and fossil data. While modest improvements to a version of the NGP salinity model were reported in Ryves (1994), other approaches offer more appropriate solutions. Firstly, it is logistically challenging to include all taxa in dissolution experiments, especially in larger, more

diverse training sets (especially as living rather than sedimentary material should be used; Ryves *et al.*, 2001). Secondly, the approach assumes that species' distribution is always a reflection of taphonomy and that dissolution state for any sample can be inferred from the taxa present (for example, downweighting samples even when assemblages consist of well preserved, but resistant taxa, due to other ecological and environmental conditions). Thirdly, the weightings themselves are arbitrary if based on relative (not absolute) resistance.

Weighting samples inversely according to dissolution state (downweighting or deleting, i.e. weight = 0) offers a direct, if blunt, approach (model E, Table 3). The underlying logic in both cases involves the assumption that poorly preserved samples are unreliable repositories of environmental information, and specifically that species optima derived from them are unsound. Downweighting samples according to dissolution index will tend to dampen the response of the model at higher salinities as there is a bias towards poor dissolution at higher salinities within the NGP dataset. If species in these samples are not represented in well-preserved saline samples their estimated WA optima will be underestimated relative to the unadjusted model. This is especially so for *C. quillensis* (important at Devils Lake in samples pre-1970) which has its greatest abundances in generally badly preserved samples (e.g. East Stump).

Salinity itself may interact with resistance to dissolution in complex ways. The greater separation of dissolution stages at lower salinity (Figure 3), and the general trend that dissolution increases with salinity independent of pH and depth (Ryves *et al.*, 2006), despite silica solubility itself declining, may also in part reflect processes of biogenic silica formation. Marine diatoms have been shown to produce silica of lower density (and so higher solubility, and lower resistance to dissolution) at higher salinity (Vrieling *et al.*, 2007), which raises the possibility that dissolution behavior is not just taxon specific but salinity-dependent too. This might have implications for ranking schemes and correction factors using data for individual species derived from a range of lakes of different salinity.

Nonetheless, results from this study suggest that approaches making use of individual dissolution state for each taxon within each sample (either by dissolution taxa or individual correction factors; models F–K in Table 3) can improve both models and reconstructions, although more complex models (e.g. with more "species", or abundances adjusted by *F* scores) may be produced. Even the correction method using *F* index scores (models J and K) is an oversimplification, as aggregate, assemblage-wide relationships between species loss and *F* index (from Ryves *et al.*, 2001) are applied. Previous work has suggested that species exhibit a range of population–dissolution relationships (Ryves, 1994), and while it may be unrealistic to evaluate these for all species in a training set or core, where only a few taxa dominate, it may be worth exploring these further (e.g. in Lake Baikal and the African Great Lakes; Battarbee *et al.*, 2005; Mackay *et al.*, 2005). In fact, recent evaluations of diverse diatom training sets have shown that models based on only a small fraction of the total dataset are as robust as the full model (e.g. only 15% of taxa for the SWAP pH dataset; Racca *et al.*, 2003). Using dissolution data to recalculate species abundance for key species, and basing new models on these, may be a fruitful approach for other, species-rich datasets, requiring evaluation of only a few correction factors.

4.3. Salinity inferences at Devils Lake and Spiritwood Lake

Incorporating dissolution data into models does lead to substantial differences in inferred salinity at both sites, particularly during more saline periods. As samples become more dissolved (driven by increasing salinity and lower lake level; Barker, 1992; Reed, 1998b; Ryves *et al.*, 2006), models making use of information on the salinity distribution of more dissolved stages within the NGP training set infer elevated salinity compared to models ignoring this (Figure 9). All salinity models can differentiate between high and low salinity events but as inferred salinity co-varies with sample dissolution state, errors are strongly correlated with sample dissolution index within the fossil assemblages (Ryves *et al.*, 2006). As preservation is generally good in the freshwater lakes within the training set, all models produce very similar results in this part of the gradient. Given the strong effect of salinity on preservation, however, in situations where salinity is perhaps not the main factor controlling dissolution, this can lead to error.

While it is unclear why preservation was poor during high lake level at the end of the 19th century at Devils Lake (leading to overestimation of inferred salinity under dissolution models), low lake level during the Dust Bowl likely had important taphonomic impacts. In this case, while dissolution models infer higher salinity than comparable unadjusted models (Figure 9A), salinity is underestimated in these very poorly preserved samples. Dissolution does destroy information and while inferences may be improved (in the sense of being nearer measured values), beyond some threshold reconstructions cannot be improved. This will depend on the proportion of robust taxa (i.e. identifiable when heavily dissolved) in the original fossil sample, the optima of which will determine the inferred salinity as dissolution progresses to an end state. Ultimately, even dissolution models will produce underestimates at high salinity as the distribution of taxa (and dissolution pseudospecies) is truncated by progressive dissolution, with optima biased to the salinity at which some preservation occurs. For this reason, even though valve counts for Alkaline and East Stump are less than 50, inclusion of these samples does allow higher salinity values to be inferred, and in some sense provides analogues with poorly preserved samples found in fossil datasets. Inclusion of these sites increased the range of theoretical salinity inference for dissolution models using pseudospecies (models G and I in Table 3) from 150 g L^{-1} TDS to >300 g L^{-1} TDS, as estimated by running a dummy sample containing a single taxon with the greatest salinity optimum for each model.

At Spiritwood Lake (Figure 9B), where dissolution appears linked to both salinity and sedimentation rate (Figures 8 and 9), including Alkaline and East Stump does seem to improve the inferences under either 53-site model (whether or not dissolution data are incorporated). Measured lake salinity in 1965 is close to values inferred under the 55-site models, and about twice that under either 53-site model (thus beyond model error), and fits best with the 55-site dissolution model (G in Table 3). Unfortunately, no measurements of lake salinity are known before 1965. Lake level was known to be low in 1950 relative to the late 19th century (Johnson, 1950), although this could support all reconstructions.

However, trends in summer conductivity of local surface waters may be good indicators of summer salinity at Spiritwood. For both the James River and Jamestown Reservoir (Figure 9B), higher conductivity in the early 1960s is followed by a sudden drop to lower values from 1965–1966 until the late 1980s (while the lack of a salinity rise at Spiritwood paralleling increasing river and reservoir conductivity in the late 1980s may be a result of lake management policies adopted in that decade; see below). If so, the higher summer conductivity recorded in the James River in the early 1950s (and so unaffected by any hydrological impacts of the Jamestown Reservoir, construction of which was not begun until 1952) lends support to model G which infers elevated lake salinity at this time compared to the other three models. If dissolution model G is accepted as being the most accurate (i.e. useful) available, it would suggest that the lake crossed the saline threshold (3 g L^{-1} TDS) by the 1940s and remained so throughout the

1950s. Spiritwood Lake may thus be more responsive to regional aridity than implied by other DI-salinity models.

Paleolimnological studies within the NGP have shown that lakes only 100–200 km apart may have distinctly different salinity histories, even to major climate events that are considered regionally synchronous (Fritz *et al.*, 2000; Laird *et al.*, 2003). Compared with Devils Lake, Spiritwood Lake (Figure 9) appears to show a damped and lagged response to the Dust Bowl drought of the 1930s–1940s, with maximum salinity values occurring in the 1950s, and slightly elevated salinity in the 1970s, perhaps in response to regional drought in the 1960s (cf. Devils Lake, Figure 7).

Groundwater (via connection to the Spiritwood Valley aquifer) likely plays an important role in modulating the chemical response to drought. Anecdotal evidence over the 20th century suggests Spiritwood Lake has never become strongly saline over this time, and it was known in pre-European Sioux folklore as a permanent source of drinking water (Johnson, 1950). Large interannual lake level changes of several meters (perhaps up to 30% lake volume) have been reported in the 20th century (Johnson, 1950), however, suggesting that the lake is sensitive to fluctuations in the annual water balance, but the diatom record implies that the inverse relationship between volume and salinity commonly assumed for closed basins does not hold here. Spiritwood Lake diatom assemblages, and hence DI-salinity, since the early 1980s may also be affected by a program of lake management, aimed at reducing the levels of phosphorus in upper, photic waters by pumping out hypolimnetic waters enriched in P (and dissolved solids) during lake stratification (M. Sauer, pers. comm.), further decoupling this link in the contemporary lake system.

4.4. Dissolution profiles and taphonomic pathways for taxa

As well as using dissolution data for adjusting inference models, dissolution profiles for individual taxa can aid interpretation of sedimentary records by providing insights into, and provoking hypotheses about, sedimentation processes and the means by which environmental signals are transferred to and preserved in sedimentary archives. Valves of different species making up the sedimentary assemblage may have travelled along different taphonomic pathways (e.g. re-working of deposits under major lake level change at Devils Lake, or different patterns of seasonality at Spiritwood Lake), which may be traced by comparison of individual species' *F* values. In addition to analogue matching (Birks *et al.*, 1990) and goodness-of-fit measures (Kingston *et al.*, 1992; Laird *et al.*, 1996a), dissolution indices also provide another means of flagging samples whose inferred values should be treated with caution (Ryves *et al.*, 2006).

Although none of the Devils Lake samples were flagged as outliers by conventional goodness-of-fit measures methods, several assemblages contained significant percentages of both freshwater (e.g. *S. niagarae*; optimum 1.24 g L^{-1} TDS and *S. minutulus*; 2.06 g L^{-1} TDS) and saline taxa (e.g. *C. quillensis*; 12.53 g L^{-1} TDS). Although major seasonal salinity changes can occur in such closed lakes, inspection of the distributions of these taxa in the NGP dataset shows there is very little overlap. Species' *F* values within the Devils Lake sequence differ markedly however, with the larger, more robust *C. quillensis* valves much less well preserved, contrary to expectation (Barker *et al.*, 1994; Ryves *et al.*, 2001; Figure 7). This suggests that the source of some of these *C. quillensis* valves in the upper part of the record may be older sediments laid down during higher salinity periods and reworked during subsequent lake filling. Reconstructions in this section may be overestimated as a result.

In earlier core sections, problems of dating, resuspension and sediment re-working may affect the diatom record during the low water stand of the 1920s–1940s, when salinities were likely highest (Fritz, 1990; Figure 7). Diatom-inferred salinity is driven by *C. quillensis* and *C. elmorei/muelleri* over this period, which have salinity optima <15 g L^{-1} TDS for all models (considered as composite species or dissolution pseudospecies). Given the poor preservation of samples in this section, it may be that taxa with higher salinity optima (e.g. *Cyclotella chochtawhatcheeana*, optimum 21.5 g L^{-1} TDS) have been preferentially removed from the record, although dissolved central areas of this taxon are distinctive. At Devils Lake, sample preservation itself may best track changing salinity (r^2 = 0.77 for *F* against log(salinity), n = 15, $p < 0.001$; Figure 7) perhaps because this is amplified by lake level change crossing critical thresholds where the additional impacts of resuspension and breakage are important. Under such conditions, recovery of the true death assemblage may be impossible, and salinity reconstructions can only reflect what remains in the assemblage, regardless of techniques to adjust or rebuild salinity models (Tables 1 and 3). Errors in reconstructed values may then be directly related to preservation state (Ryves *et al.*, 2006).

In the Spiritwood Lake core, *F* index scores for *S. minutulus* and *S. niagarae* are correlated (r +0.45, n = 16 with valve counts >10 for each, $p < 0.05$) but *S. minutulus* valves are on average better preserved than *S. niagarae* (*F* = 0.48 and 0.21 respectively) again contrary to what might be expected from gross valve morphology (Barker *et al.*, 1994). Such patterns may relate to sedimentation processes associated with each species. *S. minutulus* blooms predominantly in the spring/summer (Lund, 1950; Holland, 1969; Interlandi *et al.*, 1999), associated with low Si/P ratios following strong overturn after ice-out (and replenishment of P from the anoxic hypolimnion to the upper water column). By early summer, cells will sediment into anoxic hypolimnetic waters, providing good conditions for preservation where bioturbation and mixing are minimized. In contrast, *S. niagarae* generally has the greatest abundance during autumn (Holland, 1969; Baker and Baker, 1981), linked to turbulent conditions and higher Si/P ratio, when the major stratification period is over, with sedimentation into oxic bottom waters.

In a diatom record from the Aral Sea (Austin *et al.*, 2007), basin morphometry presents the unusual situation for a relatively shallow lake where low diatom-inferred salinity (and high lake level) is inferred at times when the assemblage is dominated by periphytic taxa (e.g. the benthic *Amphora pediculus* and epiphytic *Cocconeis neodiminuta*). Source-area habitat modeling has demonstrated this possibility (Stone and Fritz, 2004), and Austin *et al.* (2007) argue that here it reflects expansion of littoral areas in the eastern Aral basin flooded during higher lake levels (and vice versa). Although the case is not explicitly made, diatom preservation (assessed by Austin *et al.* using the *F* index) may support this argument as sample *F* scores are lower in these sections and rise when diatom-inferred salinity rises (and levels fall), dropping again at higher salinity (see Figure 3 in Austin *et al.*, 2007). This is consistent with a source of diatom valves some distance from the coring site at high lake level (and so dissolving during transport), with better preservation as littoral habitats move nearer as lake level falls, until higher salinity again reduces preservation. It might be possible to test this hypothesis using habitat-specific dissolution data: if correct, at this site one would expect periphytic forms to be, on average, less well preserved than pelagic taxa at higher lake levels (plankton sedimenting more locally, and above the coring site itself) and vice versa as levels drop. Dissolution indices can highlight differences in habitat or seasonality and shed light on questions of representatively in pelagic and benthic sedimentation in a variety of situations.

4.5. Applications to other lake types and proxies

Although these results are based on dissolution processes in lake waters dominated by Na–$MgSO_4$ (Fritz *et al.*, 1993), it is

unlikely that differences in brine type per se will alter the patterns of dissolution observed within taxa, or the relative susceptibility to dissolution between taxa. While the fundamental dissolution processes should remain the same, the rate of dissolution (and equilibrium solubility) may differ substantially between high pH, high alkalinity, saline systems and lower pH, low alkalinity freshwaters, and between waters of different brine types (Barker *et al.*, 1994). Although the relationship between alkalinity and salinity does vary between different brine types (Barker *et al.*, 1994), several other studies have found that diatom dissolution increases with salinity in a range of natural systems dominated by different salts and across a broad salinity gradient, including low salinity Mg–Ca bicarbonate Greenland lakes (Ryves *et al.*, 2006), Na–K–Mg sulphate–chloride Spanish saline lakes (Reed, 1998b) and Danish brackish coastal systems (Na–Cl; Ryves *et al.*, 2004).

Where progressively more dissolved assemblages are found at higher salinity sites, using dissolution pseudospecies can improve diatom-salinity models (Figures 3– 5, Table 3). Nonetheless, reconstruction errors can arise when dissolution in fossil samples is not primarily related to salinity (e.g. Devils Lake in the late 19th century, Figure 9A). Dissolution in itself may not be the best predictor of salinity, although salinity exerts an important control over dissolution (Reed, 1998b; Ryves *et al.*, 2006), as it is also influenced by many other site-specific factors including brine type, alkalinity (pH), lake depth, mixing regime, hydrology (e.g. water permanence and groundwater flows), sedimentation rate, degradation of the diatom frustule's organic coating (by grazers or bacteria) and frustule trace metal content (Barker *et al.*, 1994; Reed, 1998b; Ryves *et al.*, 2006; Roubeix *et al.*, 2008). The dissolution pseudospecies approach should be applicable to other diatom-salinity training sets where salinity (or a correlated variable) has some explanatory power to predict dissolution, which seems to hold true for a range of brine types, though care needs to be taken when such models are applied to fossil samples.

For this reason, approaches based on applying dissolution-based correction factors to adjust abundances (i.e. do not assume a correlation between preservation and the modeled parameter) have the greatest potential for widespread application to other biological proxies, and indeed perform best for the NGP training set (models K and J: Figure 6, Table 3). Based on a subset of the 5 dominant planktonic taxa, this approach has also been successfully used for adjusting modeled diatom–environment relationships in freshwater Lake Baikal, where dissolution is a major factor affecting assemblages within its deep, oxic water column (Ryves *et al.*, 2003), and appears to have has improved paleoenvironmental reconstructions as a result (Battarbee *et al.*, 2005; Mackay *et al.*, 2005; Mackay, 2007).

4.6. Implications of diatom dissolution for biogenic silica and diatom isotope studies

Biogenic silica and diatom abundance (concentration or flux) are often used as proxies for diatom and algal productivity, to address a range of environmental questions at a variety of spatial and temporal scales (e.g. Turner and Rabalais, 1994; Williams *et al.*, 1997; Bradshaw *et al.*, 2005). Methods for adjusting relative abundances for modeling (Equation (3)) could be applied to such studies where dissolution has had uneven effects within or between assemblages in an effort to correct these, and perhaps validated and calibrated against sedimentary algal pigment concentrations or observed data (monitored diatom abundance or chlorophyll-*a*, for example).

Dissolution may also have implications for oxygen ($\delta^{18}O$) isotope studies from biogenic silica, widely used to understand modern and past hydrological and climatic processes (Leng and Barker, 2006; Mackay *et al.*, 2008; Tyler *et al.*, 2008). Studies to date examining this issue are inconclusive, for while Moschen *et al.* (2006) found that fresh diatom valves undergoing dissolution became enriched in $\delta^{18}O$, other experiments reported no significant difference for fresh or trap material even after silica loss of up to 30% (Schmidt *et al.*, 2001). Moschen *et al.* (2006) show that diatom silica rapidly loses Si–OH groups during maturation, and hypothesize that during this dehydroxylation, O^{16} is preferentially lost. Dissolution may play an important role in this early maturation process, perhaps mediated by bacteria (Roubeix *et al.*, 2008), as even in relatively shallow freshwaters, substantial dissolution can occur (e.g. Bradshaw *et al.*, 2005), with valves showing few signs of dissolution under LM despite substantial loss of valves and biogenic silica from the assemblage (Ryves *et al.*, 2001). Re-precipitation of dissolved silica onto valves during sedimentary diagenesis (Barker *et al.*, 1994; Gasse *et al.*, 1997) may potentially also affect isotopic signals. Diatom silica $\delta^{18}O$ values from freshwater lake surface sediments across Europe do nonetheless reflect the climatic gradient, despite likely dissolution impacts which may reduce the temperature component of the signal (Tyler *et al.*, 2008).

By altering species composition, dissolution may also affect oxygen isotope signals if inter- and intra-specific vital effects exist, although where differences in $\delta^{18}O$ between different size fractions of diatoms have been reported, SEM and LM observations suggest good preservation (Swann *et al.*, 2007, 2008; but see above). Isotopic signals might also be biased by differential dissolution of diatom taxa that bloom in different seasons (e.g. *Stephanodiscus* spp.; Figure 8), where there is also a seasonal difference in lake water isotope ratios (Moschen *et al.*, 2006). Given the potential for dissolution to alter the isotopic signal from biogenic silica, and increasing awareness of its impact in diverse sediment archives (e.g. Verleyen *et al.*, 2004; Bradshaw *et al.*, 2005; Rioual and Mackay, 2005; Austin *et al.*, 2007; Figures 7 and 8), an assessment of dissolution may help interpretation of diatom oxygen (and speculatively even silicon) isotopic data.

5. Conclusions

For diatoms, dissolution indices allow preservation to be quantified and samples to be compared objectively rather than on an ad hoc basis. Sample dissolution indices can be used diagnostically (as a data screening process and to flag samples) and can be used to adjust inferential models, by supplying an objective means of weighting samples, for instance. Significant improvement in model performance can be achieved using a simple pristine/dissolved classification model (model J and K, Table 3), which need not add substantially to time taken to count samples (especially if incorporated into routine counting procedures from the outset), at the same time providing insight into the taphonomy of individual taxa and the entire assemblage. Here, diatom-salinity transfer functions incorporating dissolution data perform as well as or better than orthodox models even under internal validation, but (within the NGP) all suffer from the bias (underestimation) in reconstructed salinity at the highest salinity values. This study has also shown that there is a paucity of higher salinity sites with well-preserved diatom assemblages. Targeting such gaps (perhaps meromictic lakes; Ryves *et al.*, 2006) in the dataset can be expected to improve the transfer function at higher salinities as species parameters will be more accurate, while including even badly dissolved samples in dissolution models can improve reconstructions.

For all biological proxies, information is inevitably lost along the taphonomic pathway from living community (biocoenosis) to the death assemblage (thanatcoenosis) preserved in sedimentary archives, weakening the link between fossil data and their contemporary environment, and yet this crucial aspect that has profound implications on the quality of paleoenvi-

ronmental inference is rarely considered. Incorporating taphonomic (e.g. preservation) information from the thanatcoenosis (directly or indirectly) may help reduce the disjunction between living community and sedimentary assemblage, strengthen the link between contemporary environment and sedimentary signal, and improve our inferences of past environments. Taphonomic information is most effectively applied in conjunction with (rather than as a substitute for) ecological and sedimentological knowledge, for example in determining whether a fossil occurrence is reworked, as well as the basis for adjusting sedimentary abundances. The quantitative treatment of taphonomy can extend the range, accuracy and so usefulness of inferences of past environmental change from biological proxies.

Acknowledgments

Part of this work was carried out within NERC grant GR9/02033 to DBR and RWB, and additionally during a NERC studentship to DBR (GT4/90/ALS/28), and during the 1st LIMPACS Salinisation Workshop, Mildura, Australia, September 29th–October 4th 2004. DBR's attendance at this workshop was supported by a grant from the Carlsberg Foundation, Denmark. We also thank Steven M. Robinson, North Dakota Water Science Center, U.S. Geological Survey; Mike T. Sauer, North Dakota Department of Health, and Gene R. Van Eeckhout, North Dakota Game and Fish Department, for supplying conductivity data for Spiritwood Lake and locating other hydrological data within the USGS National Water Interface System. Kate Laird, Basil Otwell OSB and Mary Young all provided much support during fieldwork in the NGP. We thank two anonymous reviewers for *Quaternary Science Reviews* for their helpful comments and Steve Juggins for advice and support throughout the project.

References

Appleby, 2001 ◄ P. G. Appleby, Chronostratigraphic techniques in recent sediments. In: W. M. Last and J. P. Smol, Editors, *Tracking Environmental Change Using Lake Sediments: Basin Analysis, Coring, and Chronological Techniques*, *Developments in Paleoenvironmental Research* **vol. 1**, Springer, New York (2001), pp. 171–203.

Appleby and Oldfield, 1978 ◄ P. G. Appleby and F. Oldfield, The calculation of ^{210}Pb dates assuming a constant rate of supply of unsupported ^{210}Pb to the sediment, *Catena* **5** (1978), pp. 1–8.

Austin *et al.*, 2007 ◄ P. Austin, A. Mackay, O. Palagushkina and M. Leng, A high-resolution diatom-inferred palaeoconductivity and lake level record of the Aral Sea for the last 1600 yr, *Quaternary Research* **67** (2007), pp. 383–393.

Baker and Baker, 1981 ◄ K. K. Baker and A. L. Baker, Seasonal succession of the phytoplankton in the Upper Mississippi river, *Hydrobiologia* **83** (1981), pp. 295–301.

Barker, 1992 ◄ P. Barker, Differential diatom dissolution in late Quaternary sediments from Lake Manyara, Tanzania: an experimental approach, *Journal of Paleolimnology* **7** (1992), pp. 235–251.

Barker *et al.*, 1994 ◄ P. Barker, J.-C. Fontes, F. Gasse and J.-C. Druart, Experimental dissolution of diatom silica in concentrated salt solutions and implications for paleoenvironmental reconstruction, *Limnology and Oceanography* **39** (1994), pp. 99–110.

Battarbee, 2000 ◄ R. W. Battarbee, Palaeolimnological approaches to climate change, with special regard to the biological record, *Quaternary Science Reviews* **19** (2000), pp. 107–124.

Battarbee *et al.*, 1984 ◄ R. W. Battarbee, C. M. Keister and J. P. Bradbury, The frustular morphology and taxonomic relationships of *Cyclotella quillensis*, Bailey. In: D. G. Mann, Editor, *Proceedings of the Seventh International Diatom Symposium, 1982, Philadelphia*, Koeltz, Koenigstein (1984), pp. 173–184.

Battarbee *et al.*, 2005 ◄ R. W. Battarbee, A. W. Mackay, D. Jewson, D. B. Ryves and M. Sturm, Differential dissolution of Lake Baikal diatoms: correction factors and implications for palaeoclimatic reconstruction, *Global and Planetary Change* **46** (2005), pp. 75–86.

Berger, 1968 ◄ W. H. Berger, Planktonic foraminifera: selective solution and paleoclimatic interpretation, *Deep-Sea Research* **15** (1968), pp. 31–43.

Birks and Birks, 2006 ◄ H. H. Birks and H. J. B. Birks, Multi-proxy studies in palaeolimnology, *Vegetation History and Archaeobotany* **15** (2006), pp. 235–251.

Birks, 1998 ◄ H. J. B. Birks, D. G. Frey & E. S. Deevey Review #1: numerical tools in palaeolimnology – progress, potentialities, and problems, *Journal of Paleolimnology* **20** (1998), pp. 307–332.

Birks and Birks, 1980 ◄ H. J. B. Birks and H. H. Birks, *Quaternary Palaeoecology*, Edward Arnold, London (1980).

Birks *et al.*, 1990 ◄ H. J. B. Birks, J. M. Line, S. Juggins, A. C. Stevenson and C. J. F. ter Braak, Diatoms and pH reconstruction, *Philosophical Transactions of the Royal Society, London: Series B* **327** (1990), pp. 263–278.

Bradshaw *et al.*, 2005 ◄ E. G. Bradshaw, P. Rasmussen, H. Nielsen and N. J. Anderson, Mid- to late-Holocene land-use change and lake development at Dallund So, Denmark: trends in lake primary production as reflected by algal and macrophyte remains, *Holocene* **15** (2005), pp. 1130–1142.

Cameron, 1995 ◄ N. G. Cameron, The representation of diatom communities in a small acid lake, *Journal of Paleolimnology* **14** (1995), pp. 185–223.

Carvalho *et al.*, 1995 ◄ L. R. Carvalho, E. J. Cox, S. C. Fritz, S. Juggins, P. A. Sims, F. Gasse and R. W. Battarbee, Standardizing the taxonomy of saline lake *Cyclotella* spp, *Diatom Research* **10** (1995), pp. 229–240.

Conley *et al.*, 1993 ◄ D. J. Conley, C. L. Schelske and E. F. Stoermer, Modification of silica biogeochemistry with eutrophication in aquatic systems, *Marine Ecology Progress Series* **101** (1993), pp. 179–192.

Davies *et al.*, 2002 ◄ S. J. Davies, S. E. Metcalfe, M. E. Caballero and S. Juggins, Developing diatom-based transfer functions for Central Mexican lakes, *Hydrobiologia* **467** (2002), pp. 199–213.

Dixit *et al.*, 2001 ◄ S. Dixit, P. Van Cappellen and A. J. van Bennekom, Processes controlling solubility of biogenic silica and pore water build-up of silicic acid in marine sediments, *Marine Chemistry* **73** (2001), pp. 333–352.

Flower, 1993 ◄ R. J. Flower, Diatom preservation: experiments and observations on dissolution and breakage in modern and fossil material, *Hydrobiologia* **269/270** (1993), pp. 473–484.

Flower and Likhoshway, 1993 ◄ R. J. Flower, Y. V. Likhoshway, An investigation of diatom preservation in Lake Baikal. *Fifth Workshop on Diatom Algae: Diatom Algae as Indicators of Changes in Climate and Environment* (1993), pp. 77–78.

Fritz, 1990 ◄ S. C. Fritz, Twentieth-century salinity and water-level fluctuations in Devil's Lake, North Dakota: test of a diatom-based transfer function, *Limnology and Oceanography* **35** (1990), pp. 1771–1781.

Fritz *et al.*, 2000 ◄ S. C. Fritz, E. Ito, Z. C. Yu, K. R. Laird and D. R. Engstrom, Hydrologic variation in the northern Great Plains during the last two millennia, *Quaternary Research* **53** (2000), pp. 175–184.

Fritz *et al.*, 1993 ◄ S. C. Fritz, S. Juggins and R. W. Battarbee, Diatom assemblages and ionic characterization of lakes of the northern Great Plains, North America: a tool for reconstructing past salinity and climate fluctuations, *Canadian Journal of Fisheries and Aquatic Sciences* **50** (1993), pp. 1844–1856.

Fritz *et al.*, 1991 ◄ S. C. Fritz, S. Juggins, R. W. Battarbee and D. R. Engstrom, Reconstruction of past changes in salinity and climate using a diatom-based transfer function, *Nature* **352** (1991), pp. 706–708.

Gasse *et al.*, 1997 ◄ F. Gasse, P. Barker, P. A. Gell, S. C. Fritz and F. Chalié, Diatom inferred salinity in palaeolakes: an indirect tracer of climate change, *Quaternary Science Reviews* **16** (1997), pp. 547–563.

Gasse *et al.*, 1995 ◄ F. Gasse, S. Juggins and L. B. Khelifa, Diatom-based transfer functions for inferring past hydrochemical characteristics of African lakes, *Palaeogeography Palaeoclimatology Palaeoecology* **117** (1995), pp. 31–54.

Holland, 1969 ◄ R. E. Holland, Seasonal fluctuations of Lake Michigan diatoms, *Limnology and Oceanography* **14** (1969), pp. 423–436.

Hutson, 1977 ◄ W. H. Hutson, Transfer functions under no-analog conditions: experiments with Indian Ocean planktonic foraminifera, *Quaternary Research* **8** (1977), pp. 355–367.

Huxel and Petri, 1963 ◄ C. J. Huxel and L. R. Petri, *Geology and Ground Water Resources of Stutsman County, North Dakota: Part 2 – Ground Water Basin Data,* North Dakota Geological Survey, Grand Forks, North Dakota (1963).

Huxel and Petri, 1965 ◄ C. J. Huxel and L. R. Petri, *Geology and Ground Water Resources of Stutsman County, North Dakota: Part 3 – Ground Water and its Chemical Quality,* North Dakota Geological Survey, Grand Forks, North Dakota (1965).

Interlandi *et al.*, 1999 ◄ S. J. Interlandi, S. S. Kilham and E. C. Theriot, Responses of phytoplankton to varied resource availability in large lakes of the Greater Yellowstone Ecosystem, *Limnology and Oceanography* **44** (1999), pp. 668–682.

Jacobson and Engstrom, 1989 ◄ H. A. Jacobson and D. R. Engstrom, Resolving the chronology of recent lake sediments: an example from Devil's Lake, North Dakota, *Journal of Paleolimnology* **2** (1989), pp. 81–97.

Johnson, 1950 ◄ E. M. Johnson, Spiritwood Lake. *Stutsman County Record,* 1950.

Johnson, 1974 ◄ T. C. Johnson, The dissolution of siliceous microfossils in surface sediments of the eastern tropical Pacific, *Deep-Sea Research* **21** (1974), pp. 851–864.

Jongman *et al.*, 1995 ◄ R. H. G. Jongman, C. J. F. ter Braak and O. F. R. van Tongeren, *Data Analysis in Community and Landscape Ecology,* Cambridge University Press, Cambridge, England (1995).

Juggins, 1992 ◄ S. Juggins, *Diatoms in the Thames Estuary, England: Ecology, Palaeoecology, and Salinity Transfer Function,* J. Cramer, Stuttgart (1992).

Juggins, 2003 ◄ S. Juggins, *C2 User Guide. Software for Ecological and Palaeoecological Data Analysis and Visualisation* (C2 version 1. 4. 3, build 1), University of Newcastle, Newcastle upon Tyne (2003).

Kingston *et al.*, 1992 ◄ J. C. Kingston, H. J. B. Birks, A. J. Uutala, B. F. Cumming and J. P. Smol, Assessing trends in fishery resources and lake water aluminum from paleolimnological analyses of siliceous algae, *Canadian Journal of Fisheries and Aquatic Sciences* **49** (1992), pp. 116–127.

Krammer and Lange-Bertalot, 1986 ◄ K. Krammer and H. Lange-Bertalot, Bacillariophyceae. 1: Teil: Naviculaceae. In: H. Ettl, G. Gärtner, J. Gerloff, H. Heynig and D. Mollenhauer, Editors, *Süsswasserflora von Mitteleuropa, Band 2/1*, Gustav Fischer Verlag, Stuttgart/New York (1986), p. 876.

Krammer and Lange-Bertalot, 1988 ◄ K. Krammer and H. Lange-Bertalot, Bacillariophyceae. 2: Teil: Bacillariaceae, Epithemiaceae, Surirellaceae. In: H. Ettl, G. Gärtner, J. Gerloff, H. Heynig and D. Mollenhauer, Editors, *Süsswasserflora von Mitteleuropa, Band 2/2*, Gustav Fischer Verlag, Stuttgart/New York (1988), p. 596.

Krammer and Lange-Bertalot, 1991a ◄ K. Krammer and H. Lange-Bertalot,

Bacillariophyceae. 3: Teil: Centrales, Fragilariaceae, Eunotiaceae. In: H. Ettl, G. Gärtner, J. Gerloff, H. Heynig and D. Mollenhauer, Editors, *Süsswasserflora von Mitteleuropa, Band 2/3*, Gustav Fischer Verlag, Stuttgart/Jena (1991), p. 576.

Krammer and Lange-Bertalot, 1991b ◄ K. Krammer and H. Lange-Bertalot, Bacillariophyceae. 4: Teil: Achnanthaceae. In: H. Ettl, G. Gärtner, J. Gerloff, H. Heynig and D. Mollenhauer, Editors, *Süsswasserflora von Mitteleuropa, Band 2/4*, Gustav Fischer Verlag, Stuttgart, Jena (1991), p. 437.

Laird *et al.*, 2003 ◄ K. R. Laird, B. F. Cumming, S. Wunsam, J. A. Rusak, R. J. Oglesby, S. C. Fritz and P. R. Leavitt, Lake sediments record large-scale shifts in moisture regimes across the northern prairies of North America during the past two millennia, *Proceedings of the National Academy of Sciences* **100** (2003), pp. 2483–2488.

Laird *et al.*, 1996a ◄ K. R. Laird, S. C. Fritz, E. C. Grimm and P. G. Mueller, Century-scale paleoclimatic reconstruction from Moon Lake, a closed-basin lake in the northern Great Plains, *Limnology and Oceanography* **41** (1996), pp. 890–902.

Laird *et al.*, 1996b ◄ K. R. Laird, S. C. Fritz, K. A. Maasch and B. F. Cumming, Greater drought intensity and frequency before AD 1200 in the northern Great Plains, USA, *Nature* **384** (1996), pp. 552–554.

Laird *et al.*, 2007 ◄ K. R. Laird, A. Michels, C. T. L. Stuart, S. E. Wilson, W. M. Last and B. F. Cumming, Examination of diatom-based changes from a climatically sensitive prairie lake (Saskatchewan, Canada) at different temporal perspectives, *Quaternary Science Reviews* **26** (2007), pp. 3328–3343.

Leng and Barker, 2006 ◄ M. J. Leng and P. A. Barker, A review of the oxygen isotope composition of lacustrine diatom silica for palaeoclimate reconstruction, *Earth-Science Reviews* **75** (2006), pp. 5–27.

Lewin, 1961 ◄ J. C. Lewin, The dissolution of silica from diatom walls, *Geochimica et Cosmochimica Acta* **21** (1961), pp. 182–198.

Lund, 1950 ◄ J. W. G. Lund, Studies on *Asterionella formosa* Hass. II. Nutrient depletion and the spring maximum, *Journal of Ecology* **38** (1950), pp. 1–35.

Mackay, 2007 ◄ A. W. Mackay, The paleoclimatology of Lake Baikal: A diatom synthesis and prospectus, *Earth-Science Reviews* **82** (2007), pp. 181–215.

Mackay *et al.*, 2003 ◄ A. W. Mackay, R. W. Battarbee, R. J. Flower, D. H. Jewson, D. B. Ryves and M. Sturm, Assessing the potential for developing internal diatom-based transfer functions for Lake Baikal, *Limnology and Oceanography* **48** (2003).

Mackay *et al.*, 1998 ◄ A. W. Mackay, R. J. Flower, A. E. Kuzmina, L. Z. Granina, N. L. Rose, P. G. Appleby, J. F. Boyle and R. W. Battarbee, Diatom succession & pollution trends in recent sediments from Lake Baikal and their relation to atmospheric pollution and to climate change, *Philosophical Transactions of the Royal Society, London Series B* **353** (1998), pp. 1011–1055.

Mackay *et al.*, 2008 ◄ A. W. Mackay, E. Karabanov, M. J. Leng, H. J. Sloane, D. W. Morley, V. N. Panizzo, G. Khursevich and D. Williams, Reconstructing hydrological variability in Lake Baikal during MIS 11: an application of oxygen isotope analysis of diatom silica, *Journal of Quaternary Science* **23** (2008), pp. 365–374.

Mackay *et al.*, 2005 ◄ A. W. Mackay, D. B. Ryves, R. W. Battarbee, R. J. Flower, D. Jewson, P. Rioual and M. Sturm, 1000 years of climate variability in central Asia: assessing the evidence using Lake Baikal (Russia) diatom assemblages and the application of a diatom-inferred model of snow cover on the lake, *Global and Planetary Change* **46** (2005), pp. 281–297.

Moschen *et al.*, 2006 ◄ R. Moschen, A. Lucke, J. Parplies, U. Radtke and G. H. Schleser, Transfer and early diagenesis of biogenic silica oxygen isotope signals during settling and sedimentation of diatoms in a temperate freshwater lake (Lake Holzmaar, Germany), *Geochimica Et Cosmochimica Acta* **70** (2006), pp. 4367–4379.

Patrick and Reimer, 1966 ◄ R. Patrick and C. Reimer, The Diatoms of the United States, *Fragilariaceae, Eunotiaceae, Achnanthaceae, Naviculaceae* **vol. 1**, The Academy of Sciences of Philadelphia (1966).

Patrick and Reimer, 1975 ◄ R. Patrick and C. Reimer, The diatoms of the United States, *Entomoneidaceae, Cymbellaceae, Gomphonemaceae, and Epithemiaceae* vol. 2, The Academy of Sciences of Philadelphia (1975).

Pichon *et al.*, 1992 ◄ J.-J. Pichon, G. Bareille, M. Labracherie, L. D. Labeyrie, A. Baudrimont and J. -L. Turon, Quantification of the biogenic silica dissolution in Southern Ocean sediments, *Quaternary Research* **37** (1992), pp. 361–378.

Racca and Prairie, 2004 ◄ J. M. J. Racca and Y. T. Prairie, Apparent and real bias in numerical transfer functions in palaeolimnology, *Journal of Paleolimnology* **31** (2004), pp. 117–124.

Racca *et al.*, 2003 ◄ J. M. J. Racca, M. Wild, H. J. B. Birks and Y. T. Prairie, Separating wheat from chaff: diatom taxon selection using an artificial neural network pruning algorithm, *Journal of Paleolimnology* **29** (2003), pp. 123–133.

Reed, 1998a ◄ J. M. Reed, A diatom-conductivity transfer function for Spanish salt lakes, *Journal of Paleolimnology* **19** (1998), pp. 399–416.

Reed, 1998b ◄ J. M. Reed, Diatom preservation in the recent sediment record of Spanish saline lakes: implications for palaeoclimate study, *Journal of Paleolimnology* **19** (1998), pp. 129–137.

Rioual and Mackay, 2005 ◄ P. Rioual and A. W. Mackay, A diatom record of centennial resolution for the Kazantsevo Interglacial stage in Lake Baikal (Siberia), *Global and Planetary Change* **46** (2005), pp. 199–219.

Roubeix *et al.*, 2008 ◄ V. Roubeix, S. Becquevort and C. Lancelot, Influence of bacteria and salinity on diatom biogenic silica dissolution in estuarine systems, *Biogeochemistry* **88** (2008), pp. 47–62.

Ryves, 1994 ◄ D. B. Ryves, Diatom dissolution in saline lake sediments: an experimental study in the Great Plains of North America. Unpublished PhD thesis, University College London, 1994.

Ryves *et al.*, 2006 ◄ D. B. Ryves, R. W. Battarbee, S. Juggins, S. C. Fritz and N. J. Anderson, Physical and chemical predictors of diatom dissolution in freshwater and saline lake sediments in North America and West Greenland, *Limnology and Oceanography* **51** (2006), pp. 1355–1368.

Ryves *et al.*, 2004 ◄ D. B. Ryves, A. L. Clarke, P. G. Appleby, S. L. Amsinck, E. Jeppesen, F. Landkildehus and N. J. Anderson, Reconstructing the salinity and environment of the Limfjord and Vejlerne Nature Reserve, Denmark, using a diatom model for brackish lakes and fjords, *Canadian Journal of Fisheries and Aquatic Sciences* **61** (2004), pp. 1988–2006.

Ryves *et al.*, 2003 ◄ D. B. Ryves, D. H. Jewson, M. Sturm, R. W. Battarbee, R. J. Flower, A. W. Mackay and N. Granin, Quantitative and qualitative relationships between planktonic diatom communities and diatom assemblages in sedimenting material and surface sediments in Lake Baikal, Siberia, *Limnology and Oceanography* **48** (2003), pp. 1643–1661.

Ryves *et al.*, 2001 ◄ D. B. Ryves, S. Juggins, S. C. Fritz and R. W. Battarbee, Experimental diatom dissolution and the quantification of microfossil preservation in sediments, *Palaeogeography Palaeoclimatology Palaeoecology* **172** (2001), pp. 99–113.

Schmidt *et al.*, 2001 ◄ M. Schmidt, R. Botz, D. Rickert, G. Bohrmann, S. R. Hall and S. Mann, Oxygen isotopes of marine diatoms and relations to opal – a maturation, *Geochimica et Cosmochimica Acta* **65** (2001), pp. 201–211.

Shemesh *et al.*, 1989 ◄ A. Shemesh, L. H. Burckle and P. N. Froelich, Dissolution and preservation of Antarctic diatoms and the effect on the sediment thanatocoenoses, *Quaternary Research* **31** (1989), pp. 288–308.

Stoermer and Smol, 1999 ◄ E. F. Stoermer and J. P. Smol, *The Diatoms: Applications for the Environmental and Earth Sciences,* Cambridge University Press, Cambridge (1999).

Stone and Fritz, 2004 ◄ J. R. Stone and S. C. Fritz, Three-dimensional modeling of lacustrine diatom habitat areas: improving paleolimnological interpretation of planktic:benthic ratios, *Limnology and Oceanography* **49** (2004), pp. 1540–1548.

Straub, 1993 ◄ F. Straub, Diatoms and their preservation in the sediments of Lake Neuchatel (Switzerland) as evidence of past hydrological changes, *Hydrobiologia* **269** (1993), pp. 167–178.

Swann *et al.*, 2008 ◄ G. E. A. Swann, M. J. Leng, H. J. Sloane and M. A. Maslin, Isotope offsets in marine diatom delta O-18 over the last 200 ka, *Journal of Quaternary Science* **23** (2008), pp. 389–400.

Swann *et al.*, 2007 ◄ G. E. A. Swann, M. J. Leng, H. J. Sloane, M. A. Maslin and J. Onodera, Diatom oxygen isotopes: evidence of a species effect in the sediment record, *Geochemistry, Geophysics, Geosystems* **8** (2007).

Tarapchak, 1973 ◄ S. J. Tarapchak, Studies on phytoplankton distribution and indicators of trophic state in Minnesota lakes. Unpublished PhD thesis, University of Minnesota, 1973.

ter Braak and Juggins, 1993 ◄ C. J. F. ter Braak and S. Juggins, Weighted averaging partial least squares regression (WA-PLS): an improved method for reconstructing environmental variables from species assemblages, *Hydrobiologia* **269/270** (1993), pp. 485–502.

ter Braak and Šmilauer, 2002 ◄ C. J. F. ter Braak and P. Šmilauer, *Canoco for Windows,* Centre for Biometry, Wageningen (2002).

Tréguer *et al.*, 1995 ◄ P. Tréguer, D. M. Nelson, A. J. Van Bennekom, D. J. DeMaster, A. Leynaert and B. Quéguiner, The silica balance in the world ocean: a reestimate, *Science* **268** (1995), pp. 375–379.

Turner and Rabalais, 1994 ◄ R. E. Turner and N. N. Rabalais, Coastal eutrophication near the Mississippi river delta, *Nature* **368** (1994), pp. 619–621.

Tyler *et al.*, 2008 ◄ J. J. Tyler, M. J. Leng, H. J. Sloane, D. Sachse and G. Gleixner, Oxygen isotope ratios of sedimentary biogenic silica reflect the European transcontinental climate gradient, *Journal of Quaternary Science* **23** (2008), pp. 341–350.

Van Cappellen *et al.*, 2002 ◄ P. Van Cappellen, S. Dixit and J. van Beusekom, Biogenic silica dissolution in the oceans: reconciling experimental and field-based dissolution rates, *Global Biogeochemical Cycles* **16** (2002) Article no. 1075.

Verleyen *et al.*, 2004 ◄ E. Verleyen, D. A. Hodgson, P. R. Leavitt, K. Sabbe and W. Vyverman, Quantifying habitat-specific diatom production: a critical assessment using morphological and biogeochemical markers in Antarctic marine and lake sediments, *Limnology and Oceanography* **49** (2004), pp. 1528–1539.

Vrieling *et al.*, 2007 ◄ E. G. Vrieling, Q. Y. Sun, M. Tian, P. J. Kooyman, W. W. C. Gieskes, R. A. van Santen and N. Sommerdijk, Salinity-dependent diatom biosilicification implies an important role of external ionic strength, *Proceedings of the National Academy of Sciences of the United States of America* **104** (2007), pp. 10441–10446.

Warnock *et al.*, 2007 ◄ J. Warnock, R. Scherer and P. Loubere, A quantitative assessment of diatom dissolution and late quaternary primary productivity in the Eastern Equatorial Pacific, *Deep-Sea Research Part II – Topical Studies in Oceanography* **54** (2007), pp. 772–783.

Williams *et al.*, 1997 ◄ D. F. Williams, J. Peck, E. B. Karabanov, A. A. Prokopenko, V. Kravchinsky, J. King and M. I. Kuzmin, Lake Baikal record of continental climate response to orbital insolation during the past 5 million years, *Science* **278** (1997), pp. 1114–1117.

Wilson *et al.*, 1996 ◄ S. E. Wilson, B. F. Cumming and J. P. Smol, Assessing the reliability of salinity inference models from diatom assemblages: an examination of a 219-lake data set from western North America, *Canadian Journal of Fisheries and Aquatic Sciences* **53** (1996), pp. 1580–1594.

Winters, 1963 ◄ H. A. Winters, *Geology and Ground Water Resources of Stutsman County, North Dakota: Part 1 – Geology,* North Dakota Geological Survey, Grand Forks, North Dakota (1963).

Yang *et al.*, 2003 ◄ X. D. Yang, C. Kamenik, R. Schmidt and S. M. Wang, Diatom-based conductivity and water-level inference models from eastern Tibetan (Qinghai-Xizang) Plateau lakes, *Journal of Paleolimnology* **30** (2003), pp. 1–19.

Appendix 1. Supplementary information

Light microscope images (LM) and scanning electron micrographs (SEM) of dissolution stages for key taxa within the Northern Great Plains training set (from Ryves, 1994), where scale is not provided on figure, see caption for details of scale bar. Many morphologically similar taxa follow similar patterns of dissolution, such as *Cyclotella*, *Stephanodiscus* (especially larger forms), larger *Navicula* and smaller and/or finer *Nitzschia* spp. (see examples below).

Figure A1. *Amphora coffeaeformis*. a. Dissolution stage 1 (LM). Scale bar = 9 µm. b. Dissolution stage 1 (LM). Scale bar = 8 µm. c. Dissolution stage 1 (SEM). d. Dissolution stage 1 (SEM). e. Dissolution stage 1 (SEM). f. Dissolution stage 1 (SEM). g. Dissolution stage 2 (SEM).

Figure A1 (Ryves et al.)

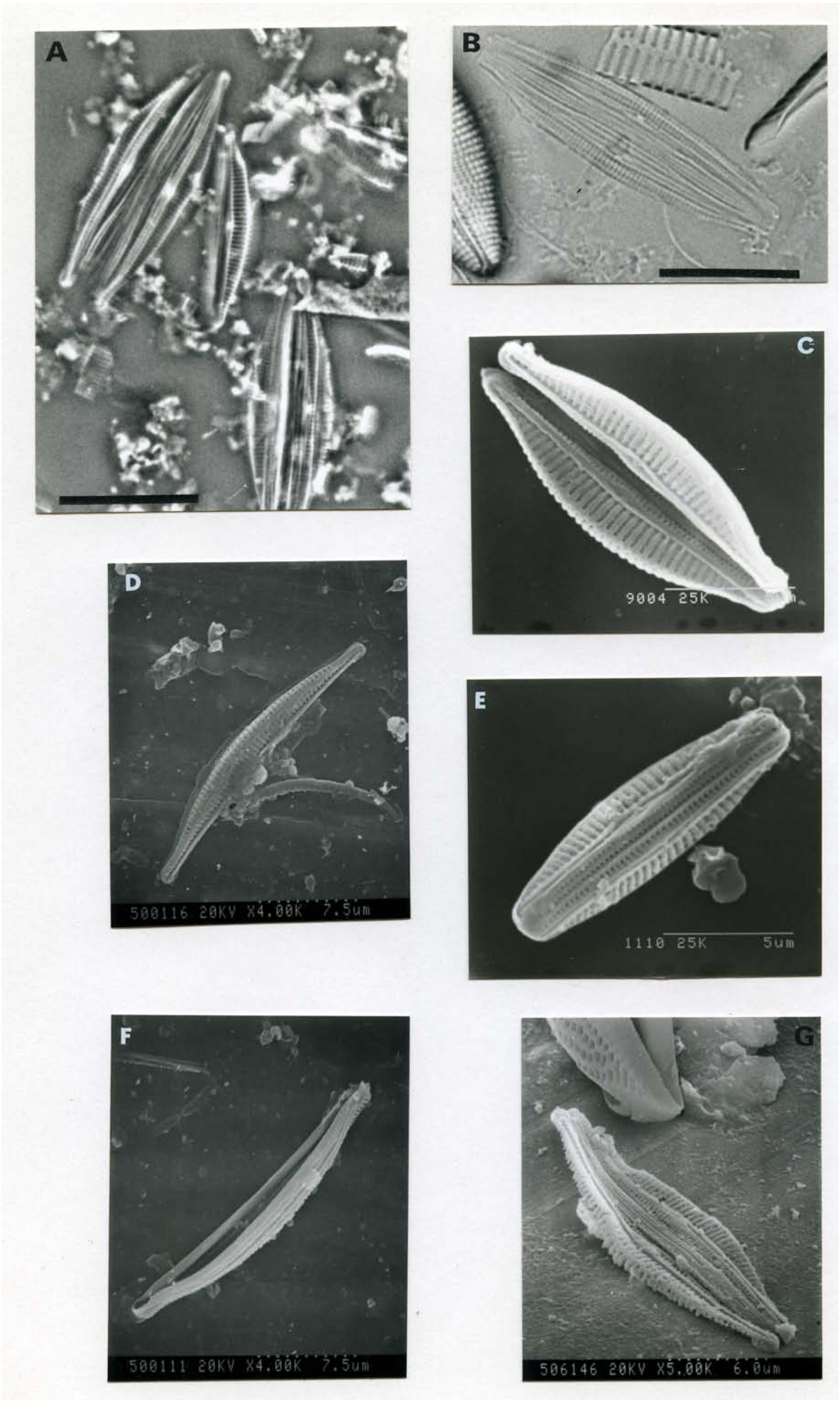

Figure A2. *Amphora libyca* (a–f) and *A. pediculus* (g). a. Dissolution stage 1 (LM) – focus A. Scale bar = 18 µm. b. Dissolution stage 1 (LM) – same valve as (a), focus B. Scale bar = 18 µm. c. Dissolution stage 1 (SEM). d. Dissolution stage 2 (SEM). Dissolution begins at valve apices. e. Dissolution stage 2 (SEM) – detail of (c). f. Dissolution stage 2 (LM). Scale bar = 16 µm. g. Dissolution stage 1 (SEM). Note "spongy" texture to frustule.

Figure A2 (Ryves et al.)

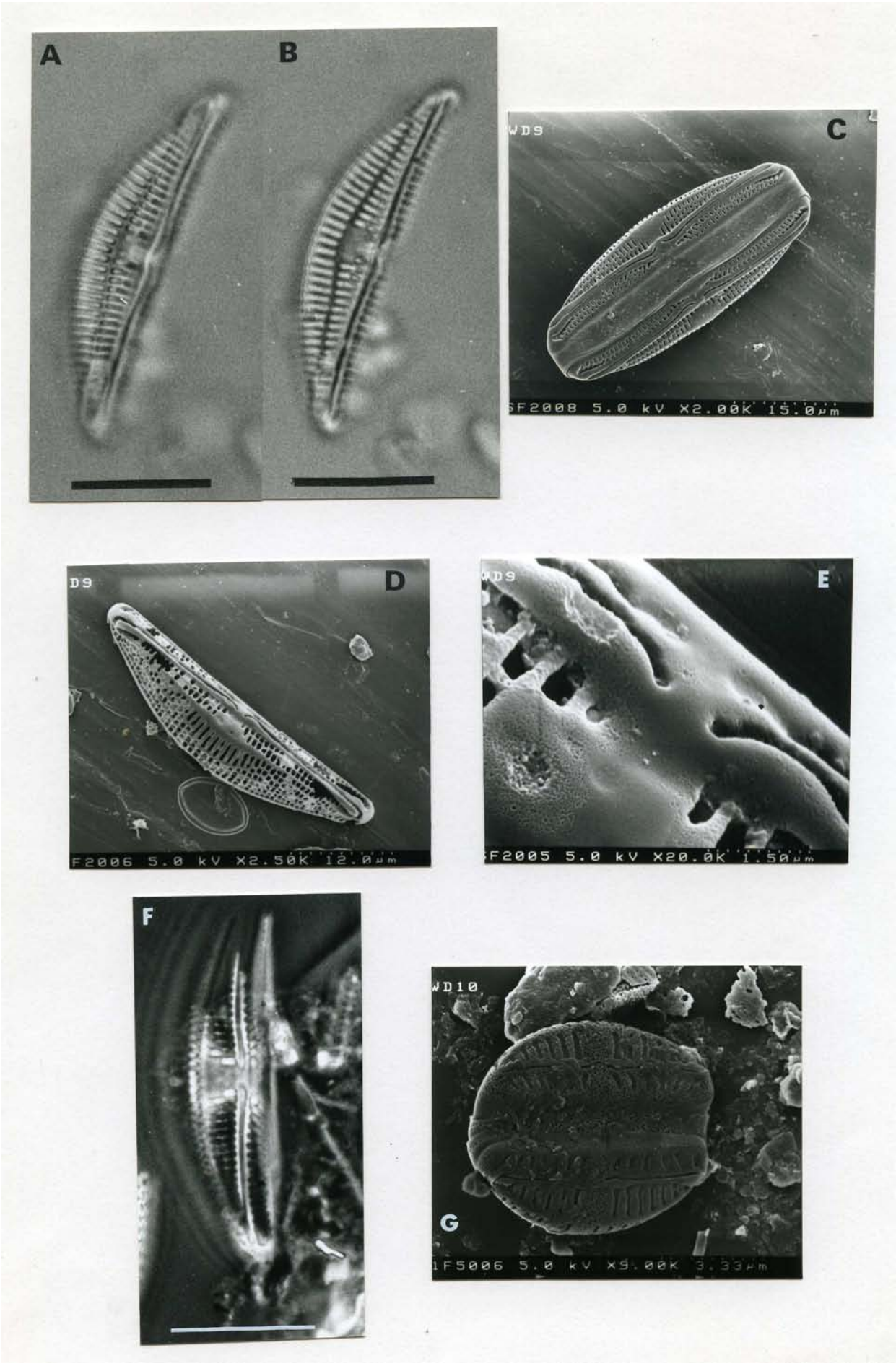

Figure A3. *Amphora libyca* (a, b) and *Brachysira aponina* (c–f). a. Dissolution stage 3 (SEM). Valve dissolves towards raphe canal, which begins to dissolve away from apices. b. Dissolution stage 4 (SEM). Raphe canal dissolves and/or breaks off, leaving a distinct central area, which is readily identifiable. c. Dissolution stage 1 (SEM). d. Dissolution stage 1 (SEM). e. Dissolution stage 1 (SEM). f. Dissolution stage 2 (SEM).

Figure A3 (Ryves et al.)

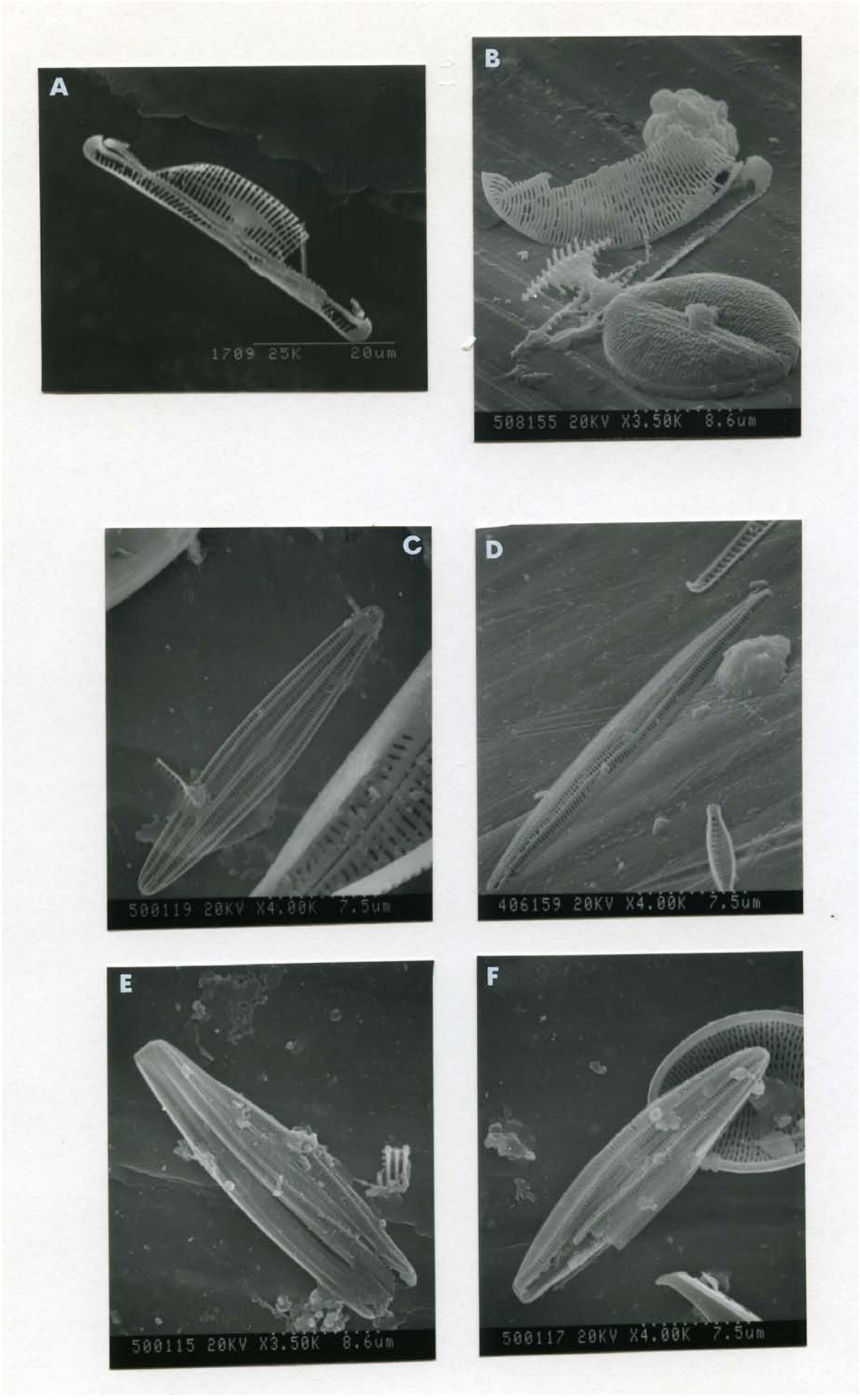

Figure A4. *Anomoeoneis costata*. a. Dissolution stage 1 (LM) – focus A. Scale bar = 15 µm. b. Dissolution stage 1 (LM) – same valve as (a), focus B. Scale bar = 15 µm. c. Dissolution stage 1 (SEM). d. Dissolution stage 2 (SEM). Detail shows dissolution around raphe and punctae enlargement. e. and f. Dissolution stage 3 (SEM). The valve may split along the raphe, which is usually the most robust structure (see f).

Figure A4 (Ryves et al.)

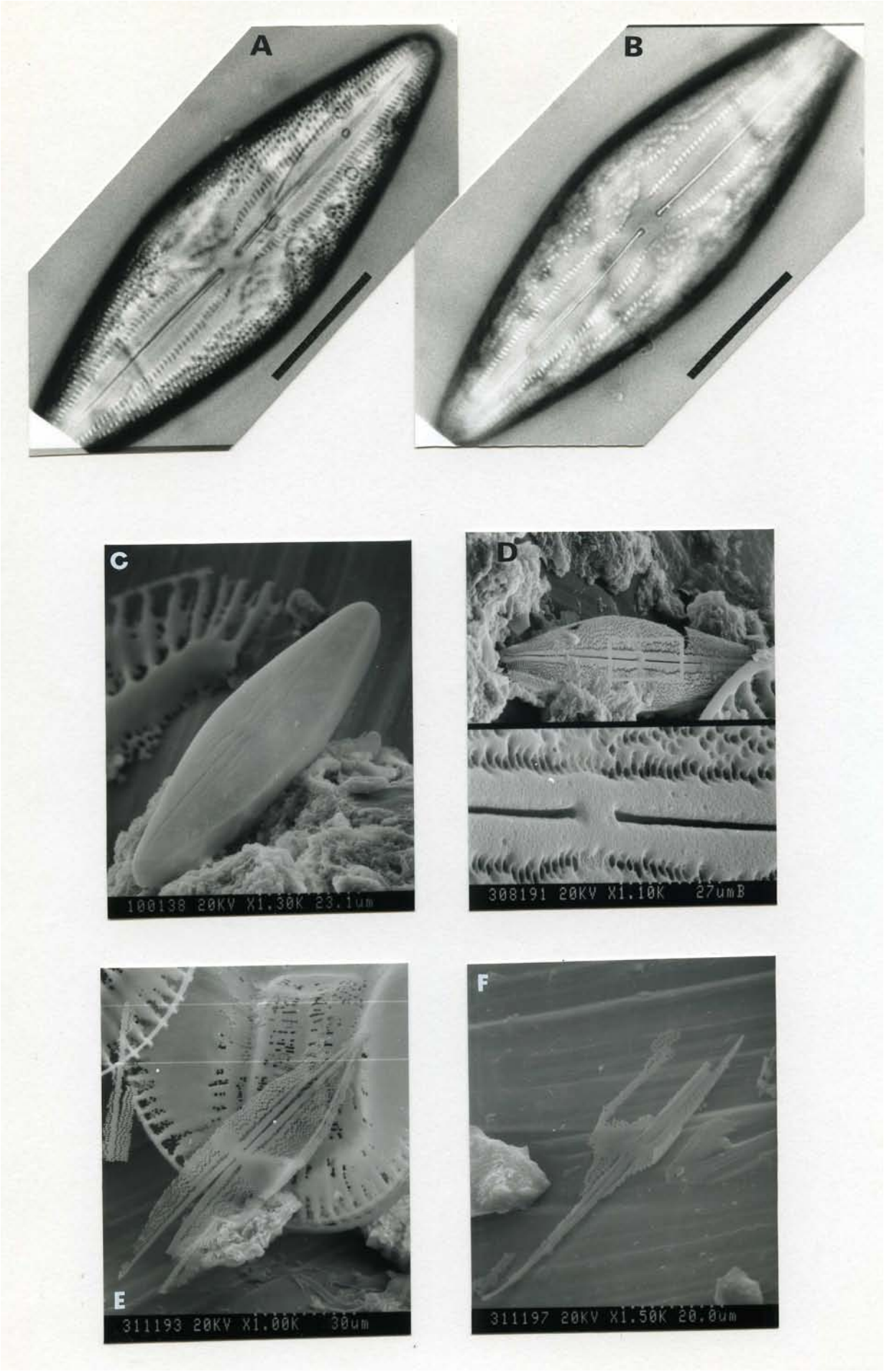

Figure A5. *Campylodiscus clypeus*. a. Dissolution stage 1 (LM). Scale bar = 45 µm. b. Dissolution stage 1 (LM). Scale bar = 40 µm. c. Dissolution stage 2 (SEM). Note corrosion of the inter-costal area at the margin. d. Dissolution stage 1 (SEM), girdle view. e. Dissolution stage 3 (SEM). The central area tends to dissolve before the thicker marginal ribs, which can be clearly seen at this stage. f. Dissolution stage 3 (SEM). The relative weakness of the central area is exploited by preferential dissolution (and breakage). Identification is by the remaining marginal ring and ribs, as the central area is usually not found whole (see c and e).

Figure A5 (Ryves et al.)

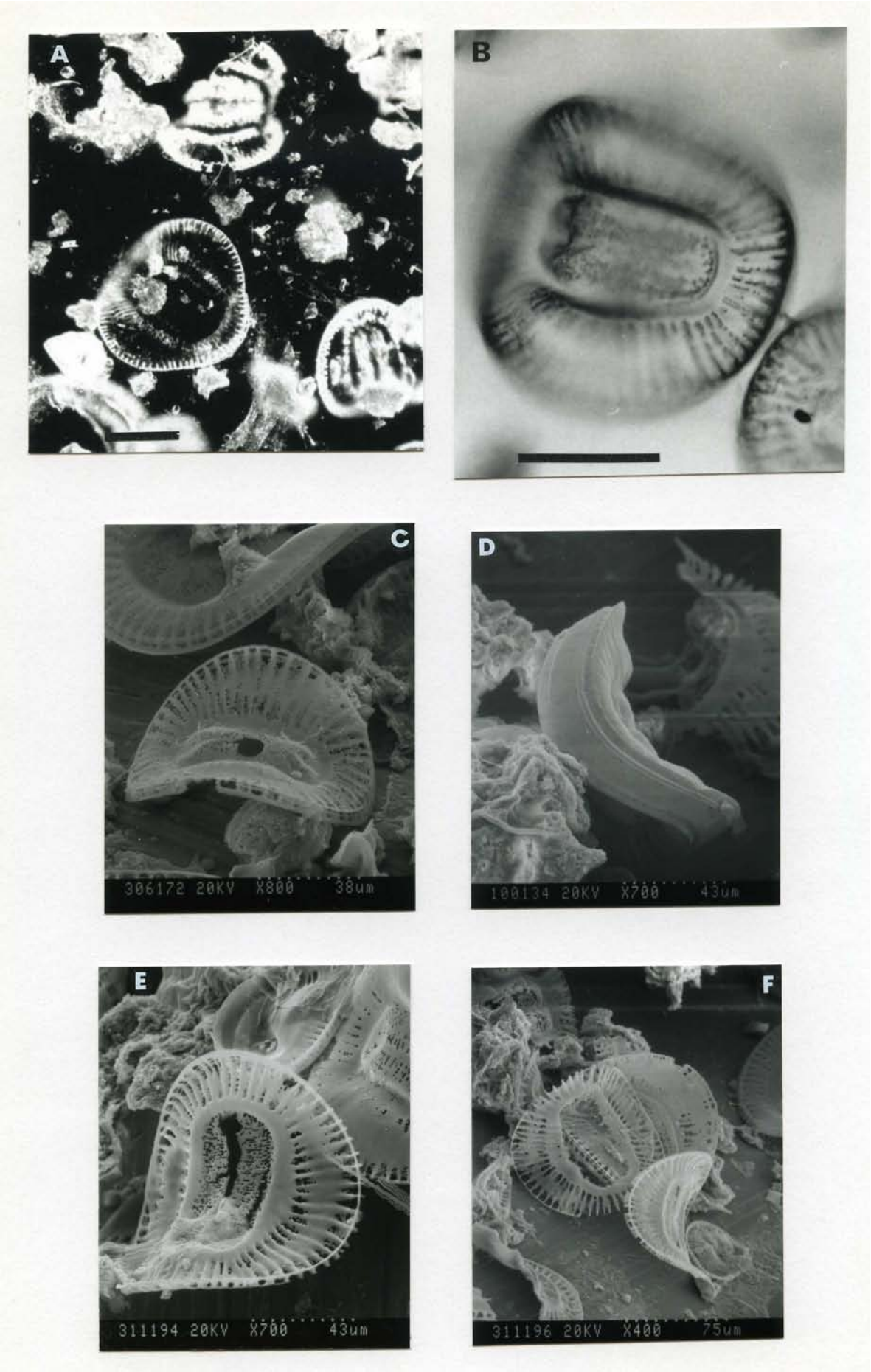

Figure A6. *Chaetoceros* [aff. *muelleri/elmorei*] vegetative cells and resting cysts. a. Fresh planktonic bloom from Coldwater Lake, live sample as collected (with a minor component of *Cyclotella quillensis*). Scale bar = 40 μm (LM). b. Fresh cells, with thin silica wall surrounding robust cyst capsule (LM). Scale bar. c. Resistant cyst, essentially featureless and heavily silicified (SEM). d. Cyst with setae intact (SEM). e. Cyst without setae (SEM). f. Cyst with setae (SEM).

Figure A6 (Ryves et al.)

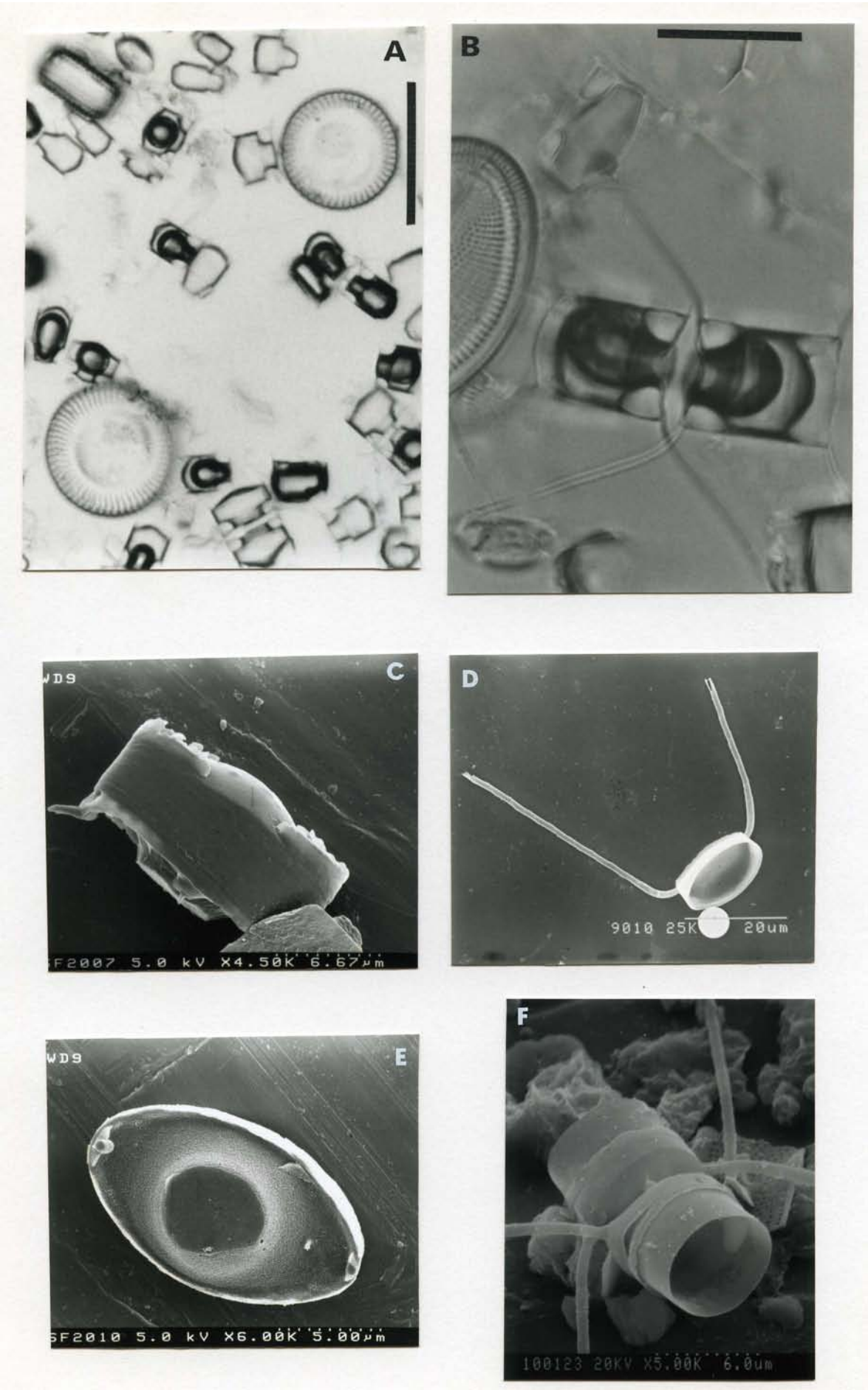

Figure A7. *Cocconeis placentula* var. *euglypta*, rapheless valve. a. Dissolution stage 1 assemblage (LM). Scale bar = 20 µm. b. Dissolution stage 1, external view (SEM). c. Dissolution stage 1, internal view (SEM). d. Dissolution stage 1, internal view (SEM). e. Dissolution stage 1, with breakage (LM). Scale bar = 10 µm. f. Dissolution stage 2 (SEM). g. Dissolution stage 2 (LM). Scale bar = 5 µm.

Figure A7 (Ryves et al.)

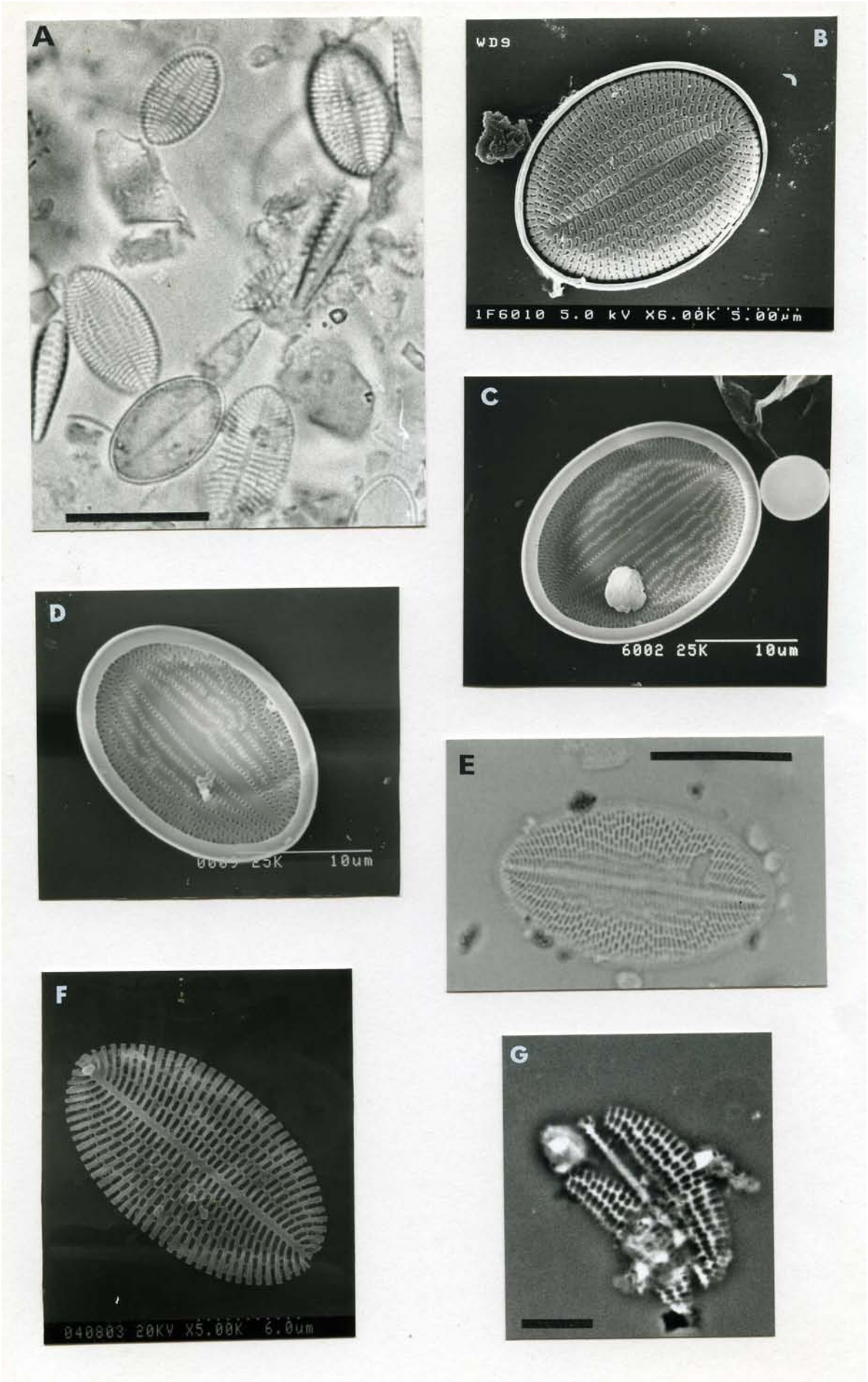

Figure A8. *Cocconeis placentula* var. *euglypta*, raphid valve. a. Dissolution stage 1 (LM). Scale bar = 5 μm. b. Dissolution stage 1 (SEM). c. Dissolution stage 1 (SEM). d. Dissolution stage 1 with signs of areolae enlargement (SEM). e. Dissolution stage 2 (SEM). f. Mantle separated from valve during dissolution (SEM).

Figure A8 (Ryves et al.)

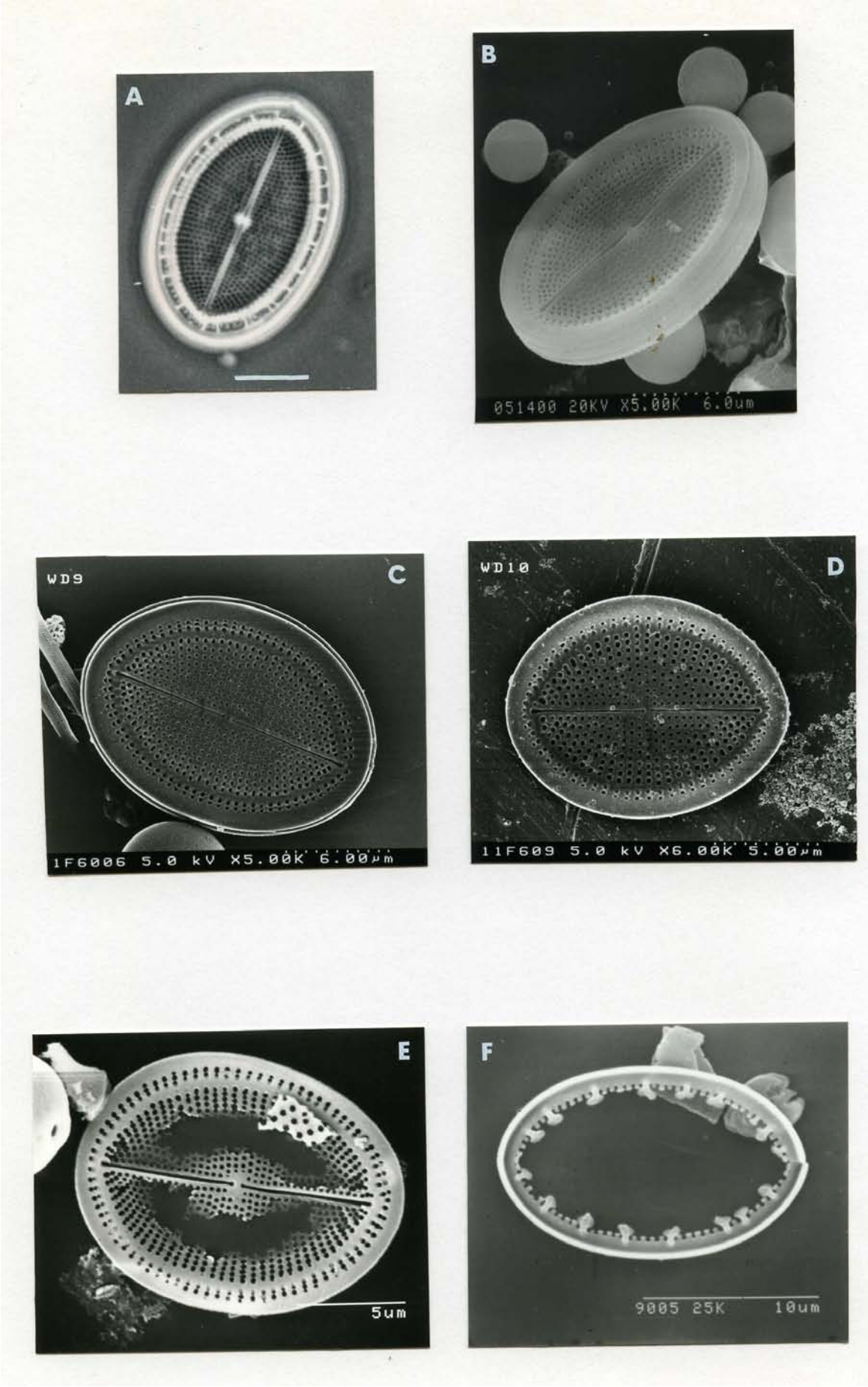

Figure A9. *Cocconeis pediculus,* rapheless valve. a. Dissolution stage 1 (LM). Scale bar = 5 µm. b. Dissolution stage 1 (LM). Scale bar = 5 µm. c. Dissolution stage 1 (LM). Scale bar = 4 µm. d. Dissolution stage 1 (SEM). e. Dissolution stage 1 (SEM). f. Dissolution stage 2 (SEM).

Figure A9 (Ryves et al.)

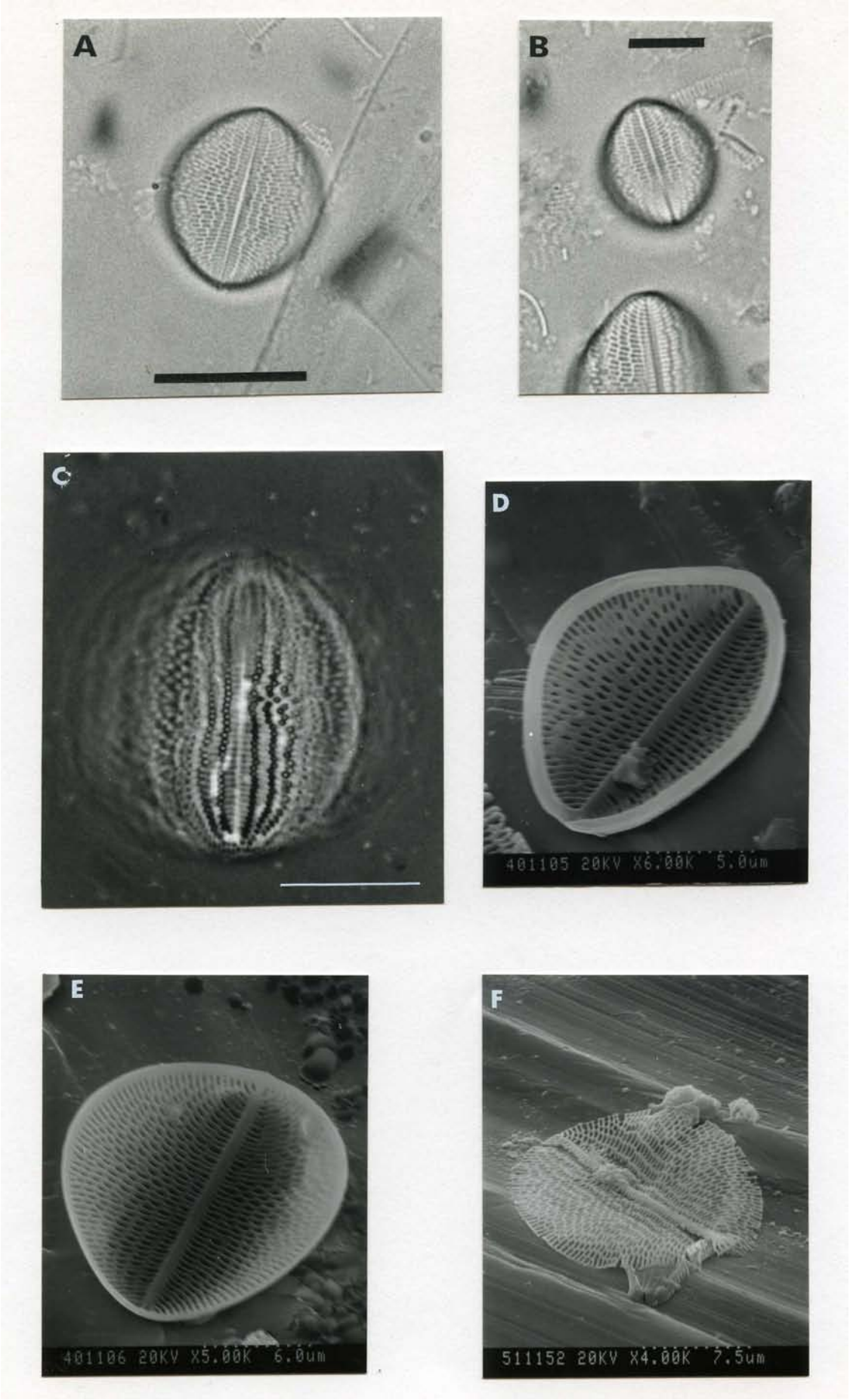

Figure A10. *Cocconeis pediculus*, raphid valve. a. Dissolution stage 1 (LM). Scale bar = 5 μm. b. Dissolution stage 1 (SEM). c. Dissolution stage 1 (SEM). d. Dissolution stage 1 (SEM). Breakage is often initiated along the apical axis. e. Dissolution stage 1 (SEM), as (d). f. Dissolution stage 2 (SEM).

Figure A10 (Ryves et al.)

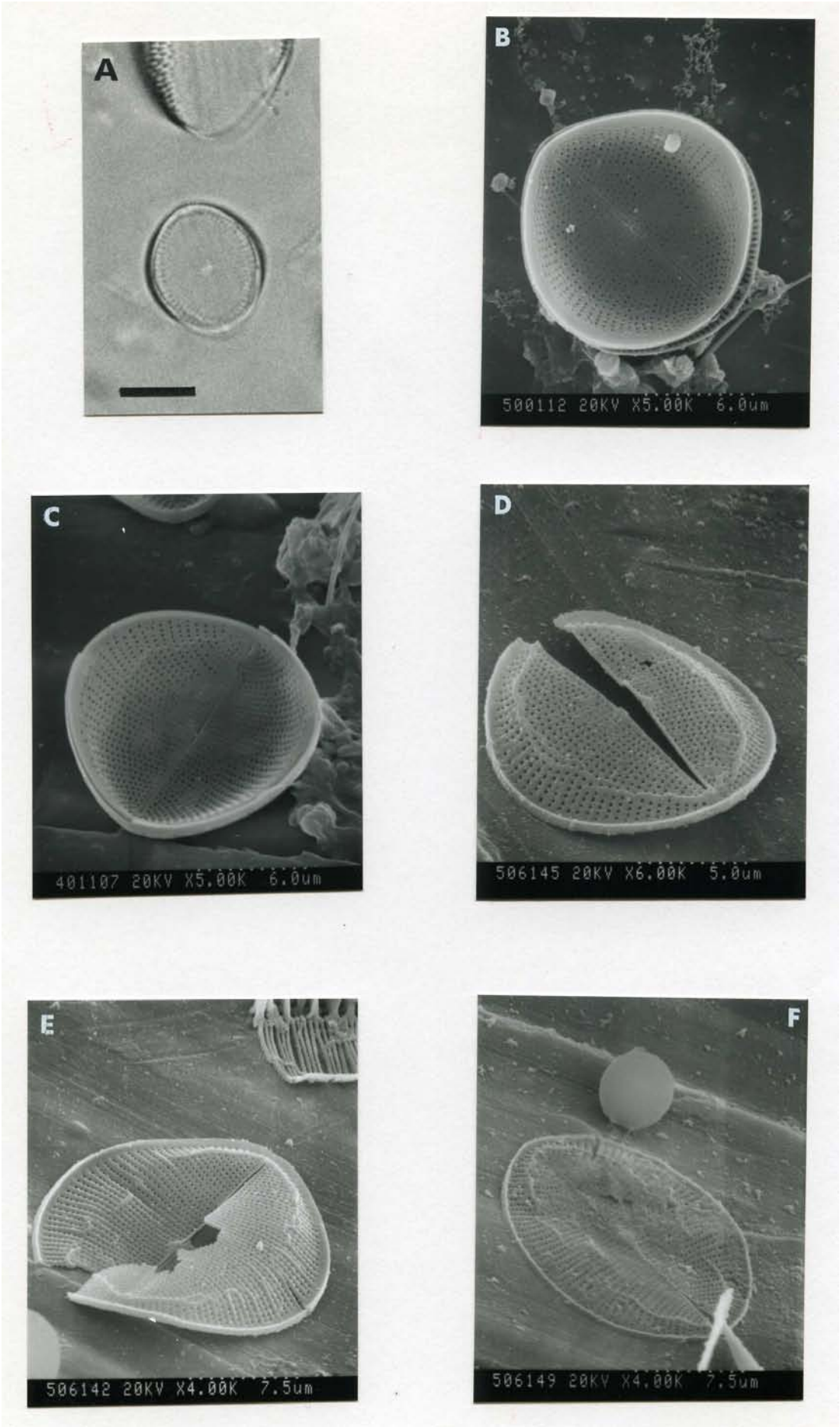

Figure A11. *Cyclotella chochtawhatcheeana*. a. Dissolution stage 1 (LM). Scale bar = 5 µm. b. Dissolution stage 1 (LM). Scale bar = 10 µm. c. Dissolution stage 1 (SEM). d. Dissolution stage 1 (SEM). e. Dissolution stage 3 (SEM). f. Dissolution stage 3 (SEM).

Figure A11 (Ryves et al.)

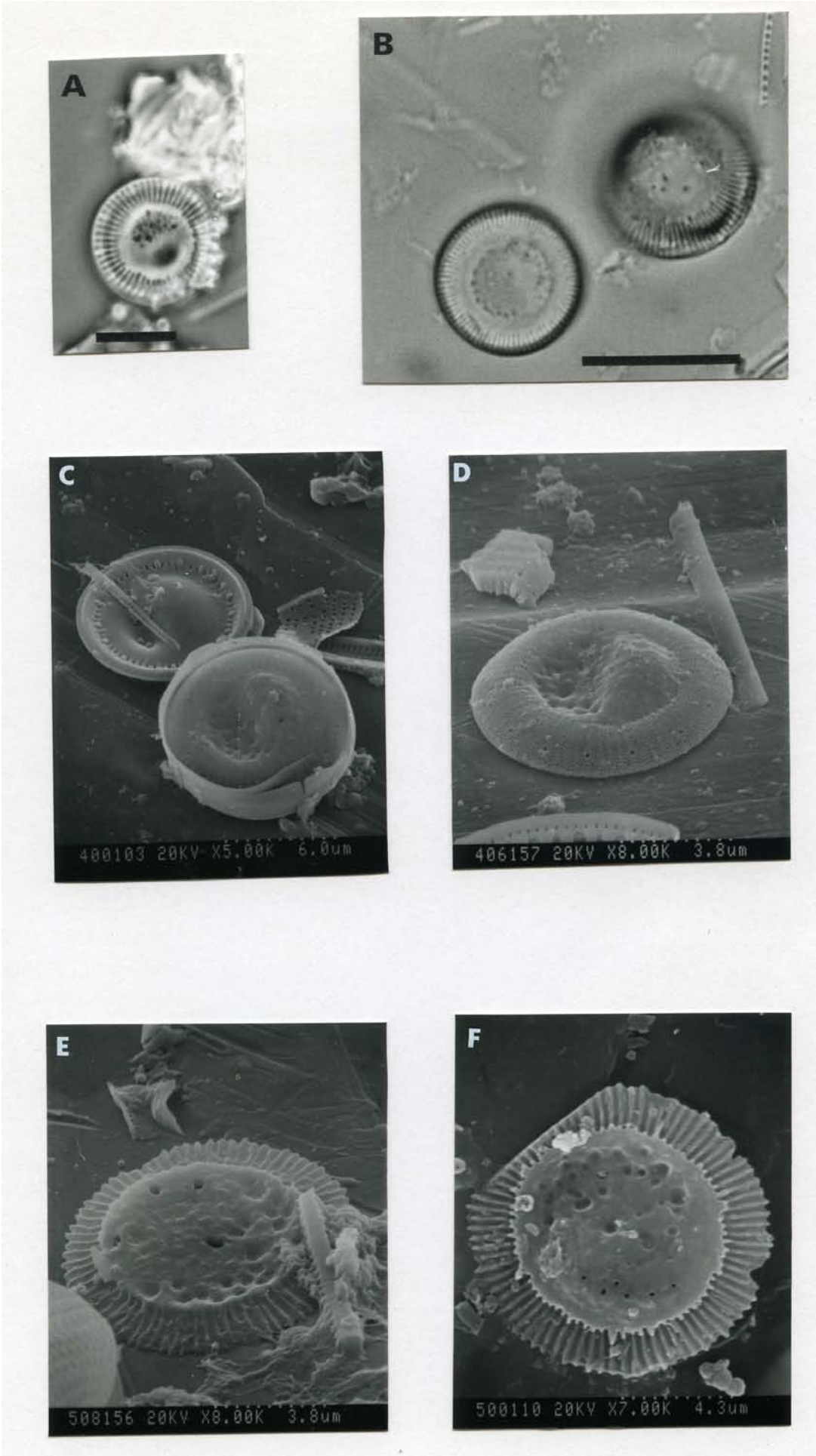

Figure A12. *Cyclotella meneghiniana*. a. Dissolution stage 1 (LM). Scale bar = 8 μm. b. Dissolution stage 1 (SEM). Detail shows structure of process (internal view). c. Dissolution stage 2 (SEM), with the outer margin complete. d. Dissolution stage 3 (SEM), with outer ring absent, but costae intact. e. Dissolution stage 3 (SEM). f. Dissolution stage 3 (LM). Scale bar = 4 μm. g. Dissolution stage 4 (SEM). Only the central silica disc remains. This is a common end stage for *Cyclotella* taxa.

Figure A12 (Ryves et al.)

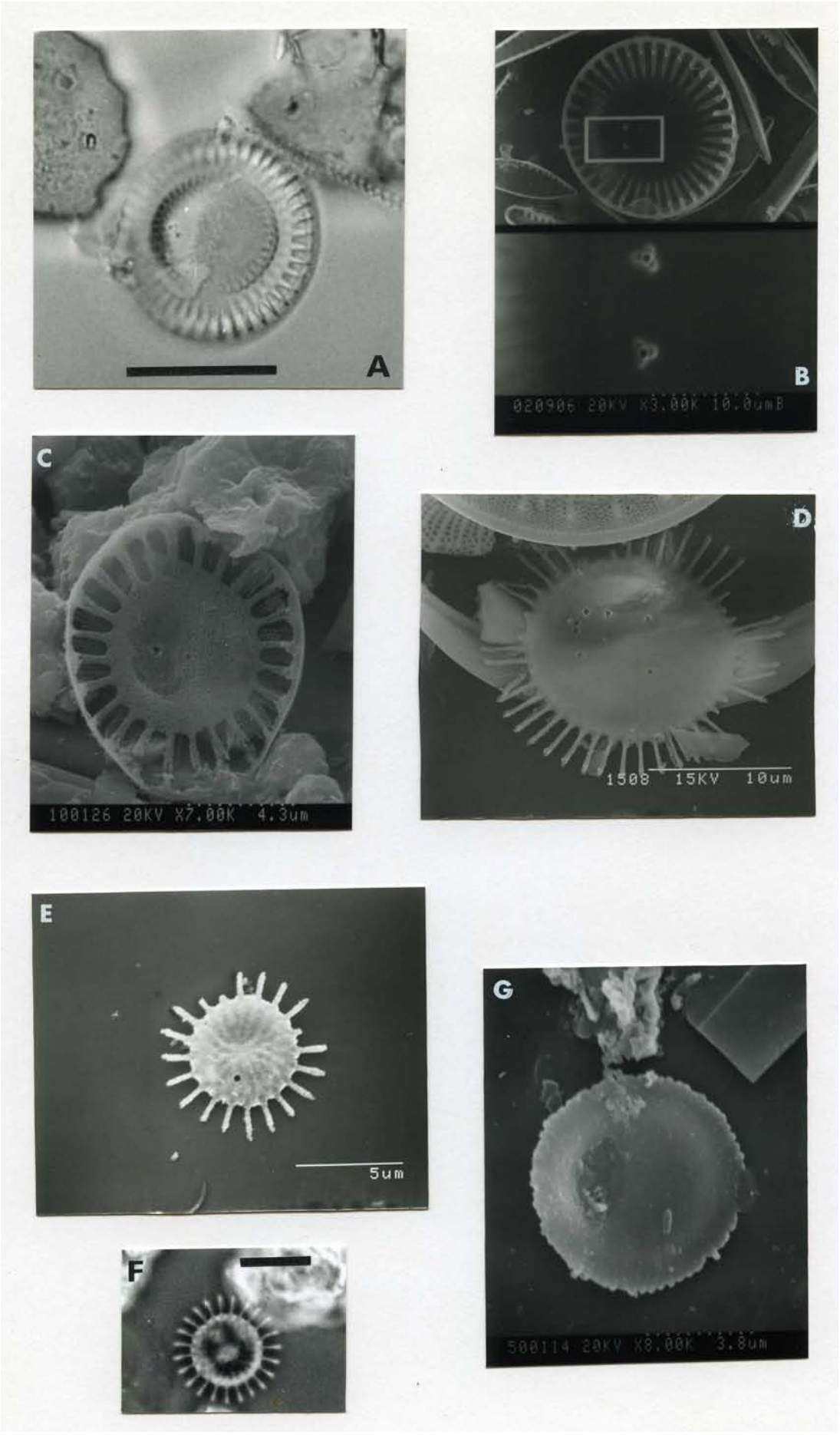

Figure A13. *Cyclotella quillensis*. a. Fresh plankton sample, dissolution stage 1 (LM) – focus A. Scale bar = 20 µm. b. Fresh plankton sample, dissolution stage 1 (LM) – same valve as (a), focus B, showing valvar undulation. Scale bar = 20 µm. c. Dissolution stage 3 (LM) – focus A. Scale bar = 10 µm. d. Dissolution stage 3 (LM) – same valve as (c), focus B. Scale bar = 10 µm. e. Dissolution stage 4 (SEM). f. Dissolution stage 4 (SEM), with stage 3 for *Amphora libyca*.

Figure A13 (Ryves et al.)

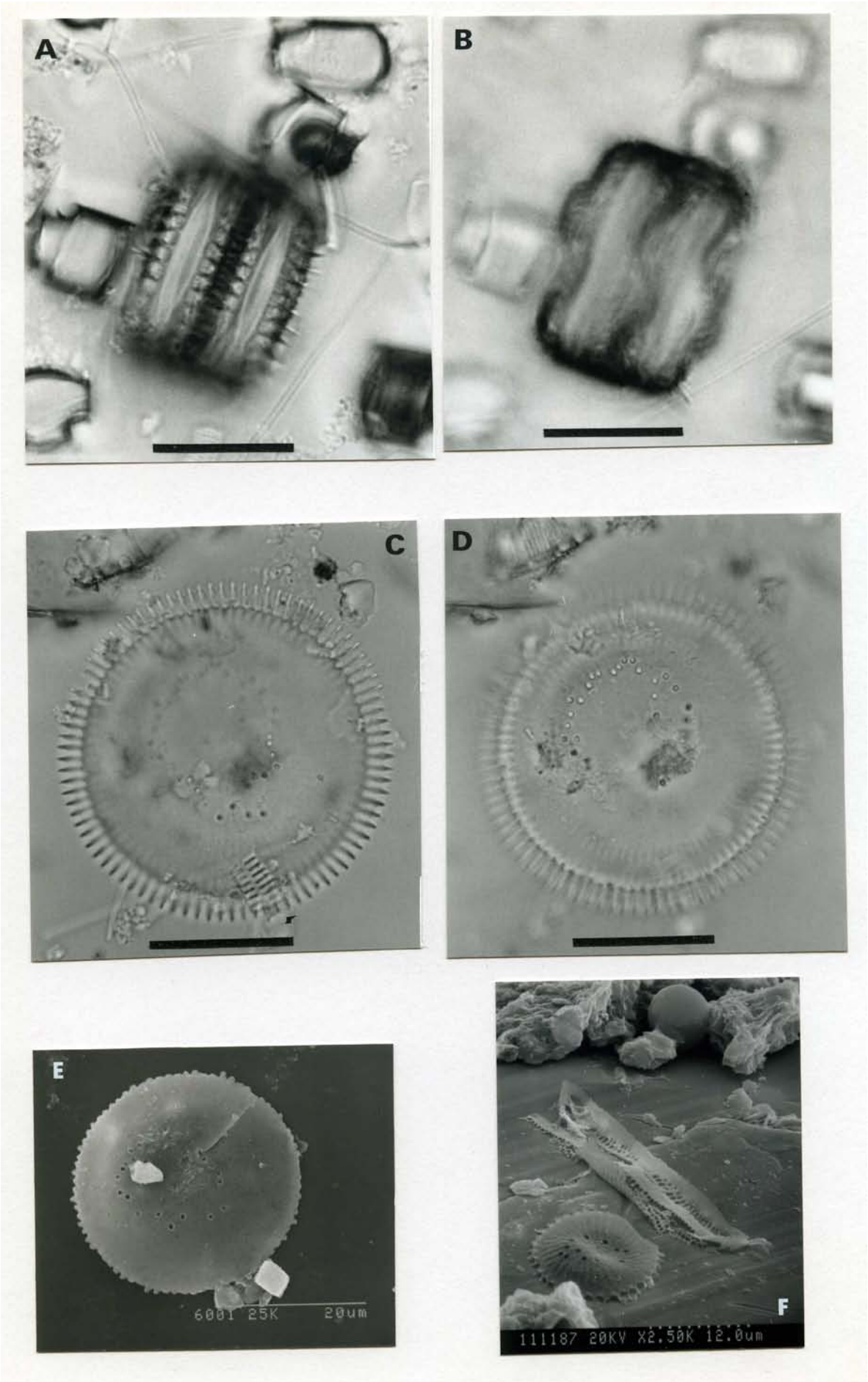

Figure A14. *Cymbella pusilla* (a–d) and *C. cistula* (e, f). a. Fresh plankton sample, dissolution stage 1 (LM). Scale bar = 10 μm. b. Dissolution stage 1, external view (SEM). c. Dissolution stage 1 (SEM), with some dissolution of internal structures (detail). d. Dissolution stage 2 (SEM), with apical degradation. e. Dissolution stage 1 (SEM). f. Dissolution stage 3 (SEM).

Figure A14 (Ryves et al.)

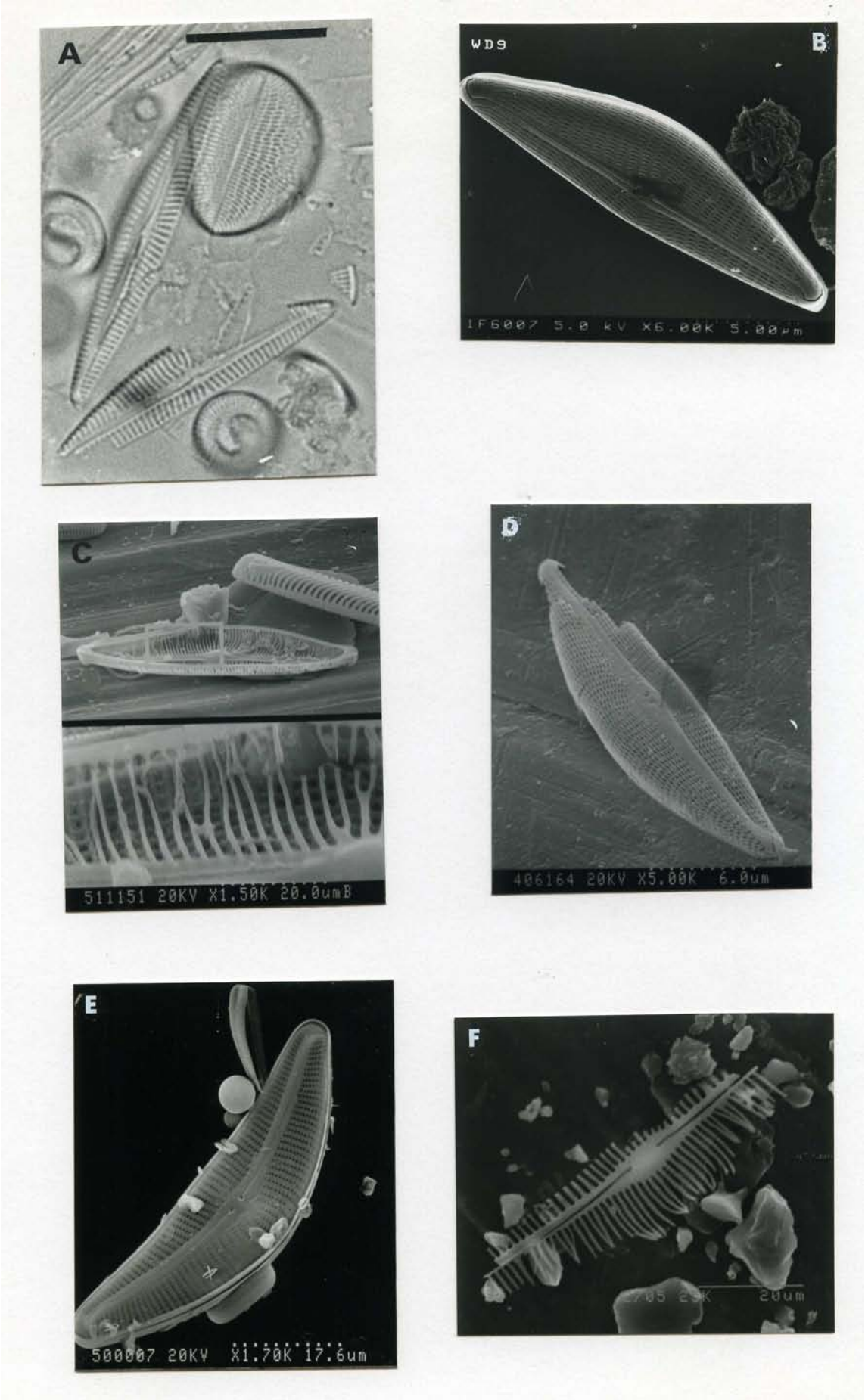

Figure A15. *Mastogloia elliptica* var. *dansei* (a–e) and *M. smithii* var. *lacustris* (f, g). a. Dissolution stage 1 (LM) – focus A. Scale bar = 12 µm. b. Dissolution stage 1 (LM) – same valve as (a), focus B. Scale bar = 12 µm. c. Dissolution stage 2 (LM). Scale bar = 12 µm. d. Dissolution stage 3 (SEM). e. Dissolution stage 4 (SEM). Only the distinctive central area remains. f. Dissolution stage 1 (SEM). g. Dissolution stage 2 (SEM).

Figure A15 (Ryves et al.)

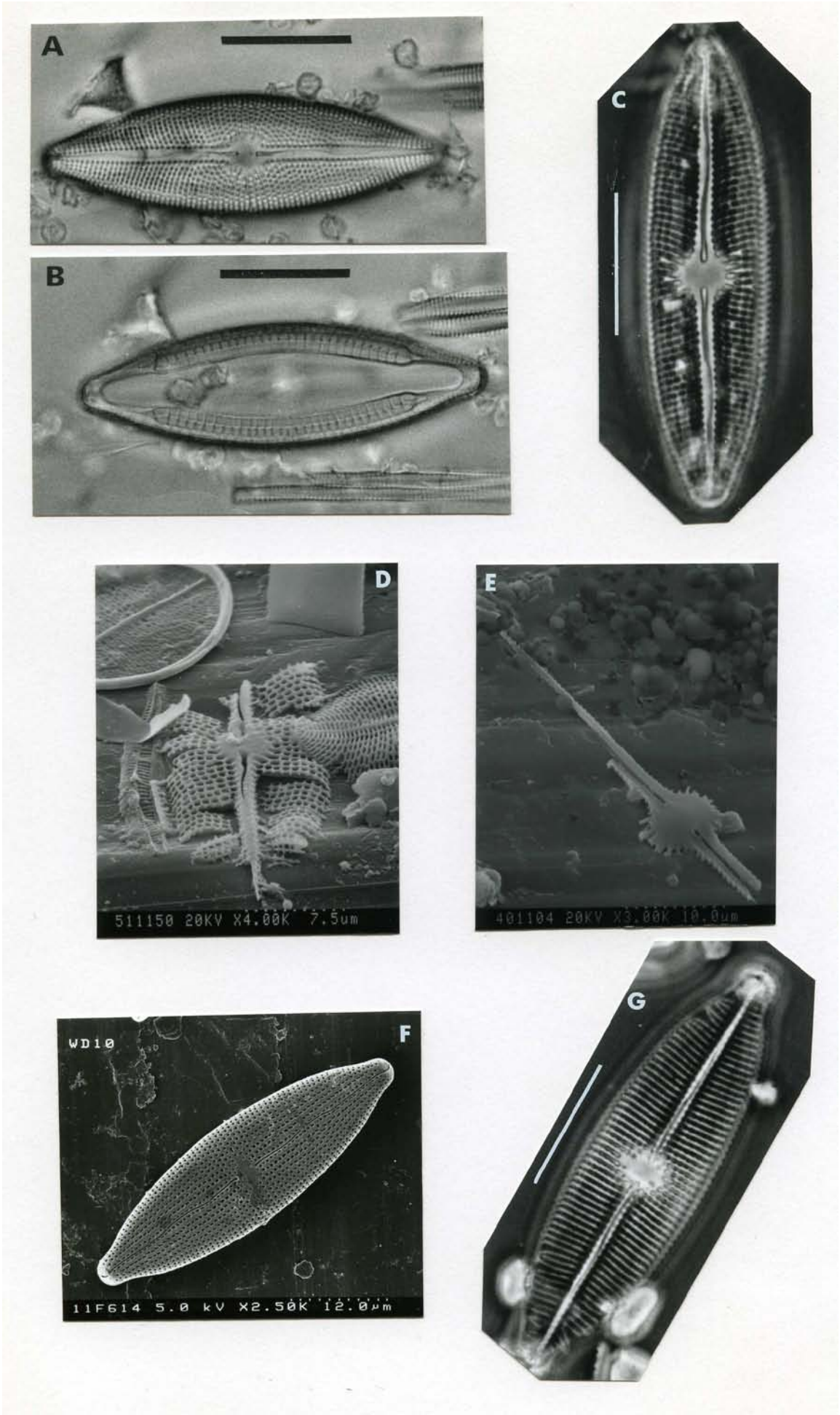

Figure A16. *Navicula oblonga*. Similar patterns are observed with many other pennate taxa with a relatively unornamented, thickened and so robust central area. a. Dissolution stage 1 (SEM). b. Dissolution stage 2 (SEM). Vela within striae dissolve. c. Dissolution stage 2 (SEM), detail of (b). d. Dissolution stage 2 (SEM), with detail of striae dissolution of internal structures within striae. e. Dissolution stage 3 (SEM). Dissolution proceeds from the apices to the central area. f. Dissolution stage 4 (LM). Robust central area allows identification often to species level for larger taxa. Scale bar = 10 μm. g. Dissolution stage 4 (SEM). h. Dissolved end of valve, distinct for *N. oblonga*, but this often breaks up along raphe. Identification is thus preferably based upon central areas (f, g) (SEM).

Figure A16 (Ryves et al.)

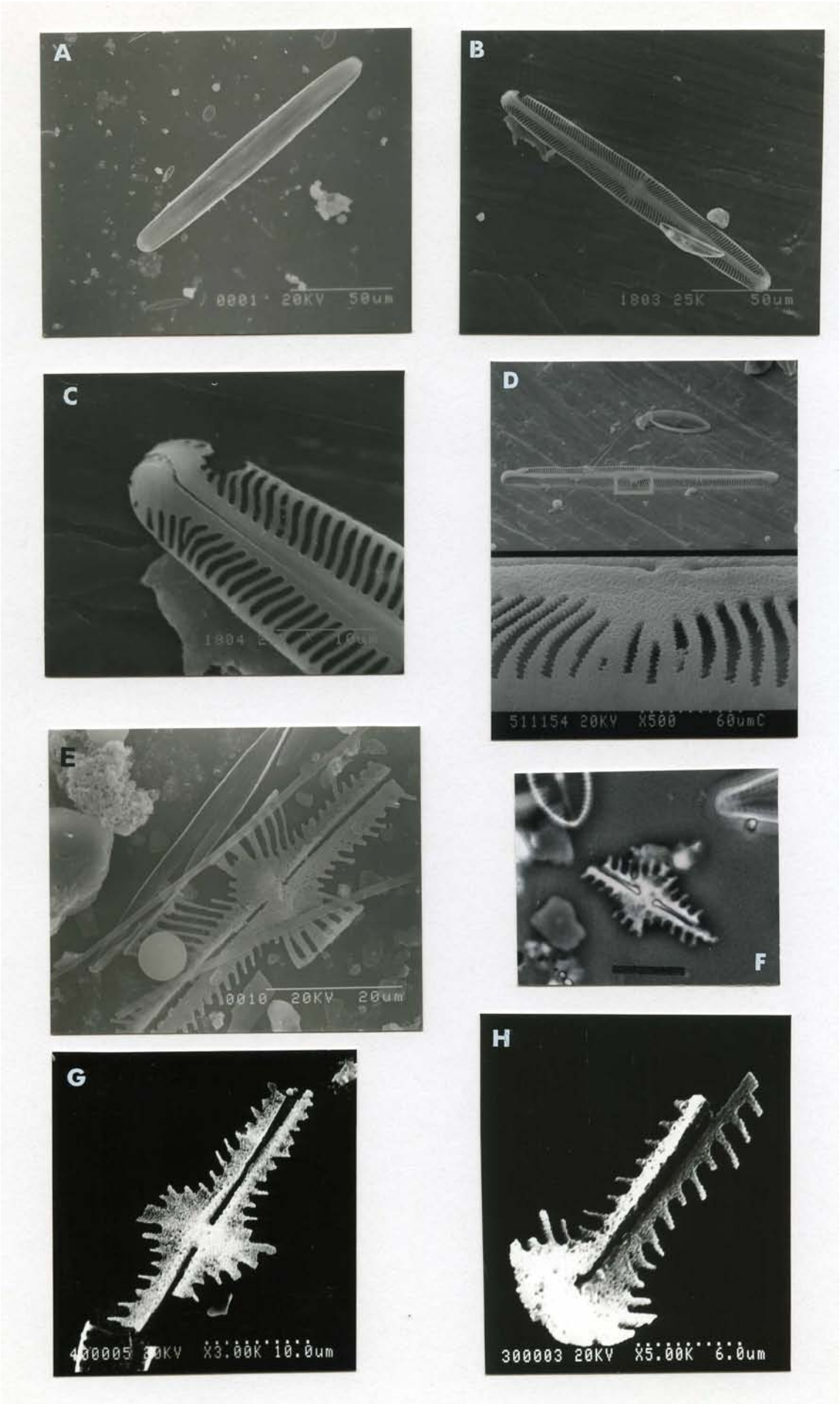

Figure A17. *Nitzschia palea* (a, f, g) and *N. frustulum* (b–e, h). a. Dissolution stage 1 (LM). Scale bar = 10 µm. b. Dissolution stage 1 (LM). Scale bar = 3 µm. c. Dissolution stage 1 (LM). Scale bar = 5 µm. d. Dissolution stage 1 (SEM). e. Dissolution stage 1 (SEM). f. Detail of valve dissolution (SEM). g. Dissolution stage 2 (SEM). h. Dissolution stage 2 (SEM).

Figure A17 (Ryves et al.)

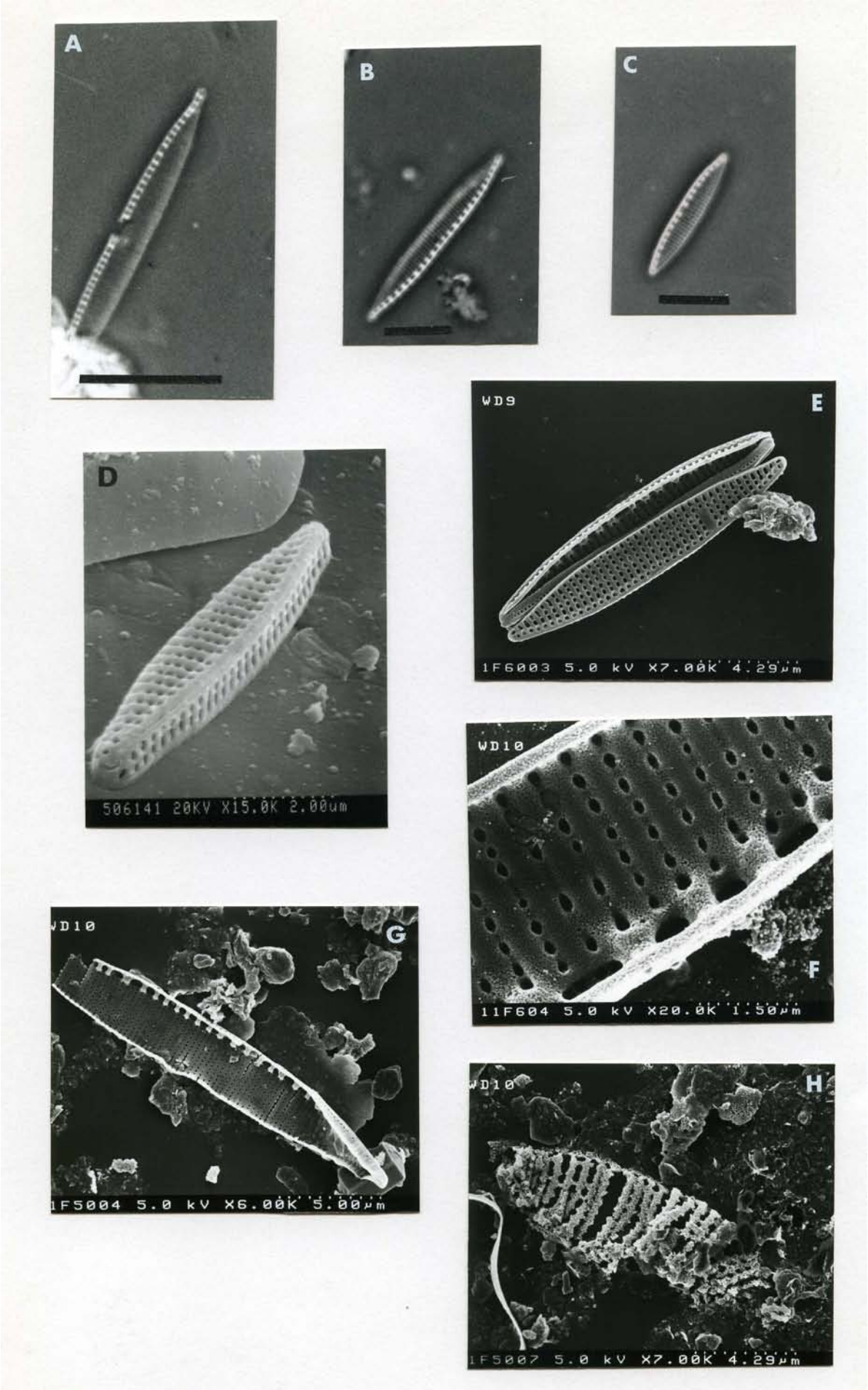

Figure A18. *Rhoicosphenia curvata* (a–d) and Rhopalodia gibba (e, f). a. Dissolution stage 1 (LM), girdle view. Scale bar = 15 μm. b. Dissolution stage 1 (SEM), whole cell in girdle view. c. Dissolution stage 1 (SEM), rapheless valve. d. Dissolution stage 2 (SEM), rapheless valve. e. Dissolution stage 1 (SEM). f. Dissolution stage 2 (SEM), with loss of valve ends. g. Dissolution stage 1 (LM). Scale bar = 10 μm.

Figure A18 (Ryves et al.)

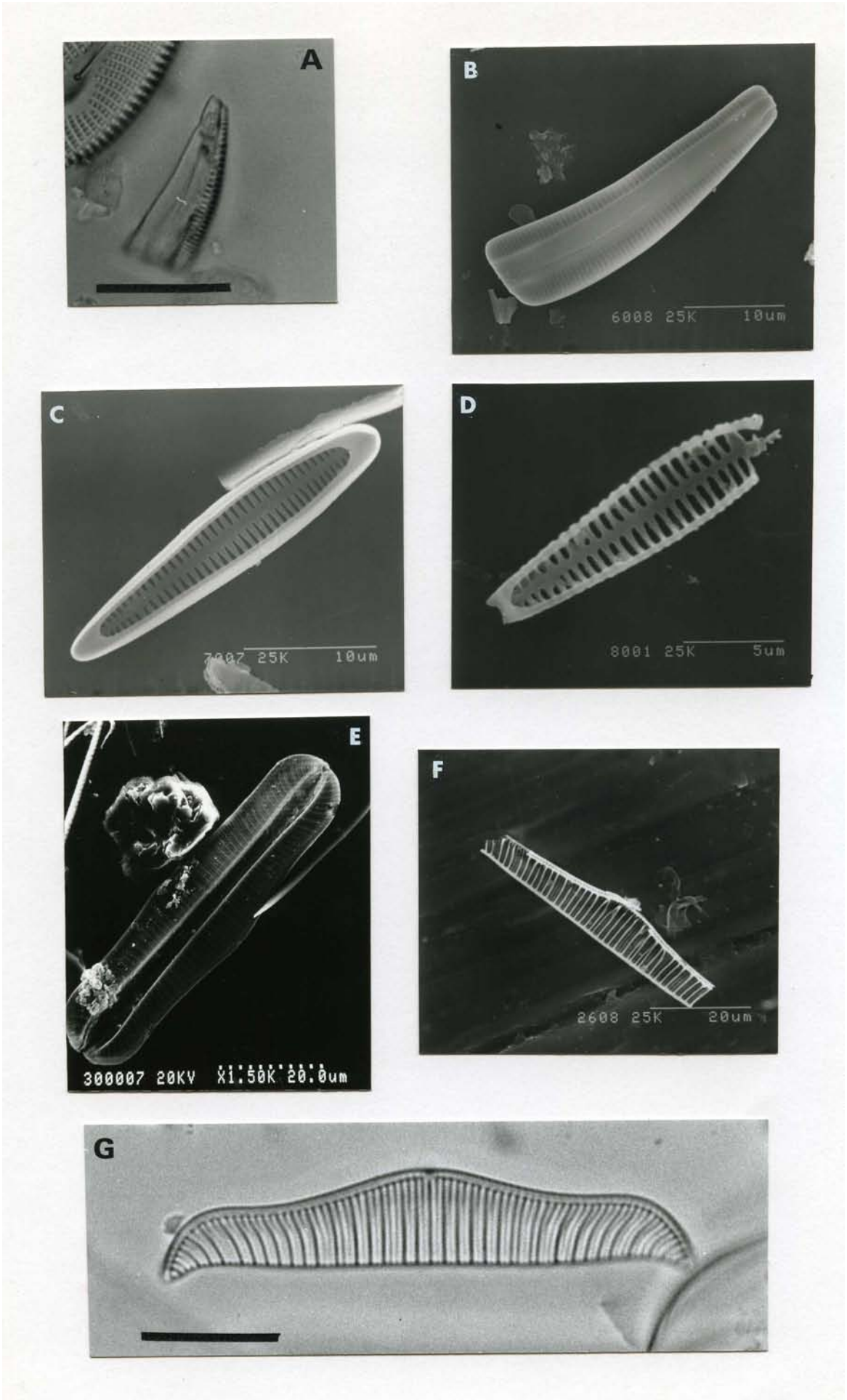

Figure A19. *Stephanodiscus minutulus*. a. Dissolution stage 1 (LM) – focus A. Scale bar = 3 µm. b. Dissolution stage 1 (LM) – same valve as (a), focus B. Scale bar = 3 µm. c. Dissolution stage 1 (LM) – focus A. Scale bar = 3 µm. d. Dissolution stage 1 (LM) – same valve as (c), focus B. Scale bar = 3 µm. f. Dissolution stage 1 (SEM), external view. g. Dissolution stage 1 (SEM), internal view. h. Dissolution stage 1 (SEM), with some dissolution evident. i. Dissolution stage 2 (SEM), with vestigial marginal spines. j. Dissolution stage 2 (SEM), as (i). k. Dissolution stage 3 (SEM), with complete loss of marginal spines.

Figure A19 (Ryves et al.)

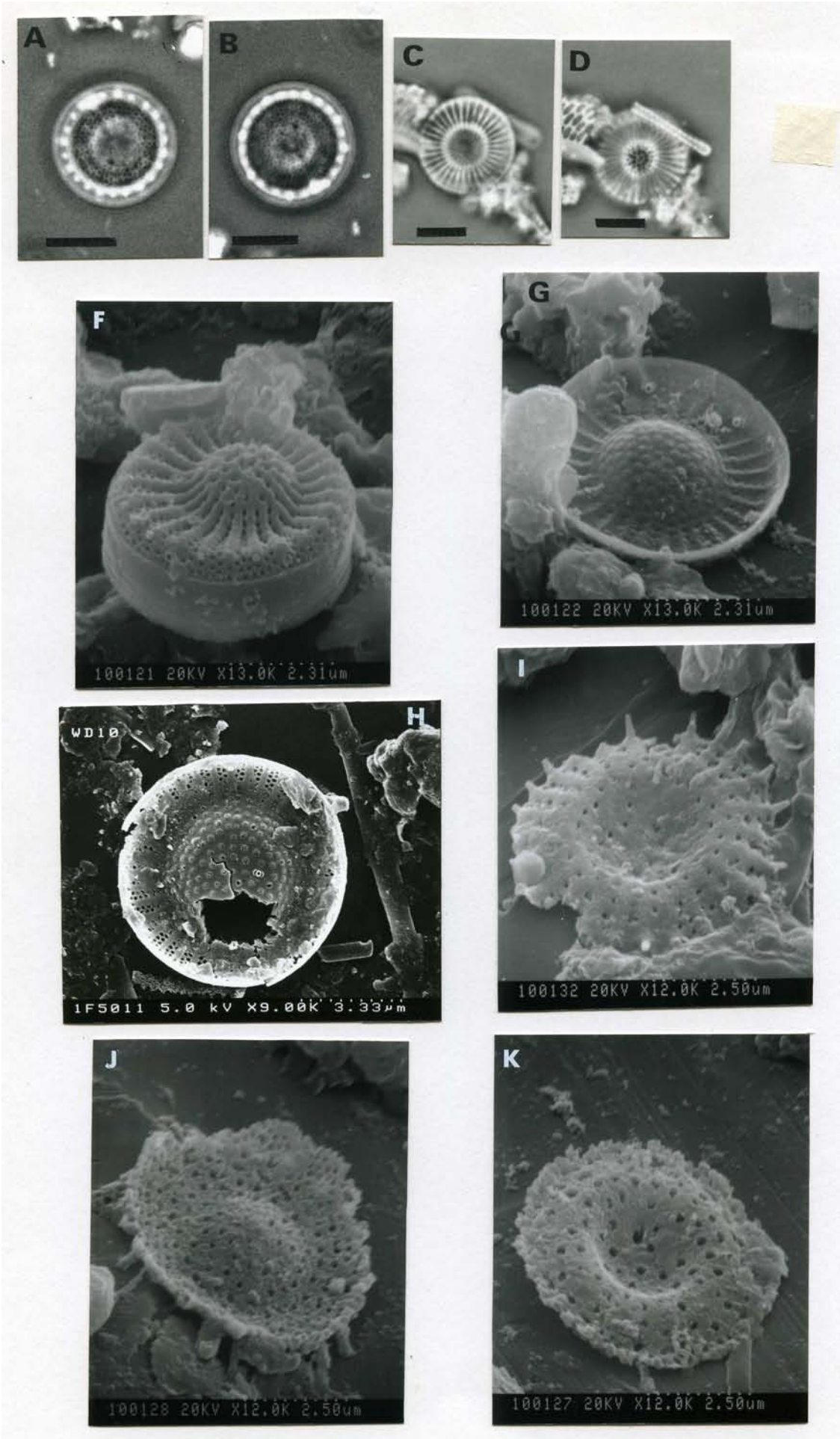

Figure A20. *Stephanodiscus niagarae*. a. Dissolution stage 1 (LM). Scale bar = 8 μm. b. Dissolution stage 1 (SEM), with some dissolution. c. Dissolution stage 1 (SEM), with detail of areolae (internal view). d. Dissolution stage 2 (SEM), showing loss of structural integrity. e. Dissolution stage 3 (SEM). Note the loss of marginal spines – cf. (b). f. Dissolution stage 3 (SEM); as (e).

Figure A20 (Ryves et al.)

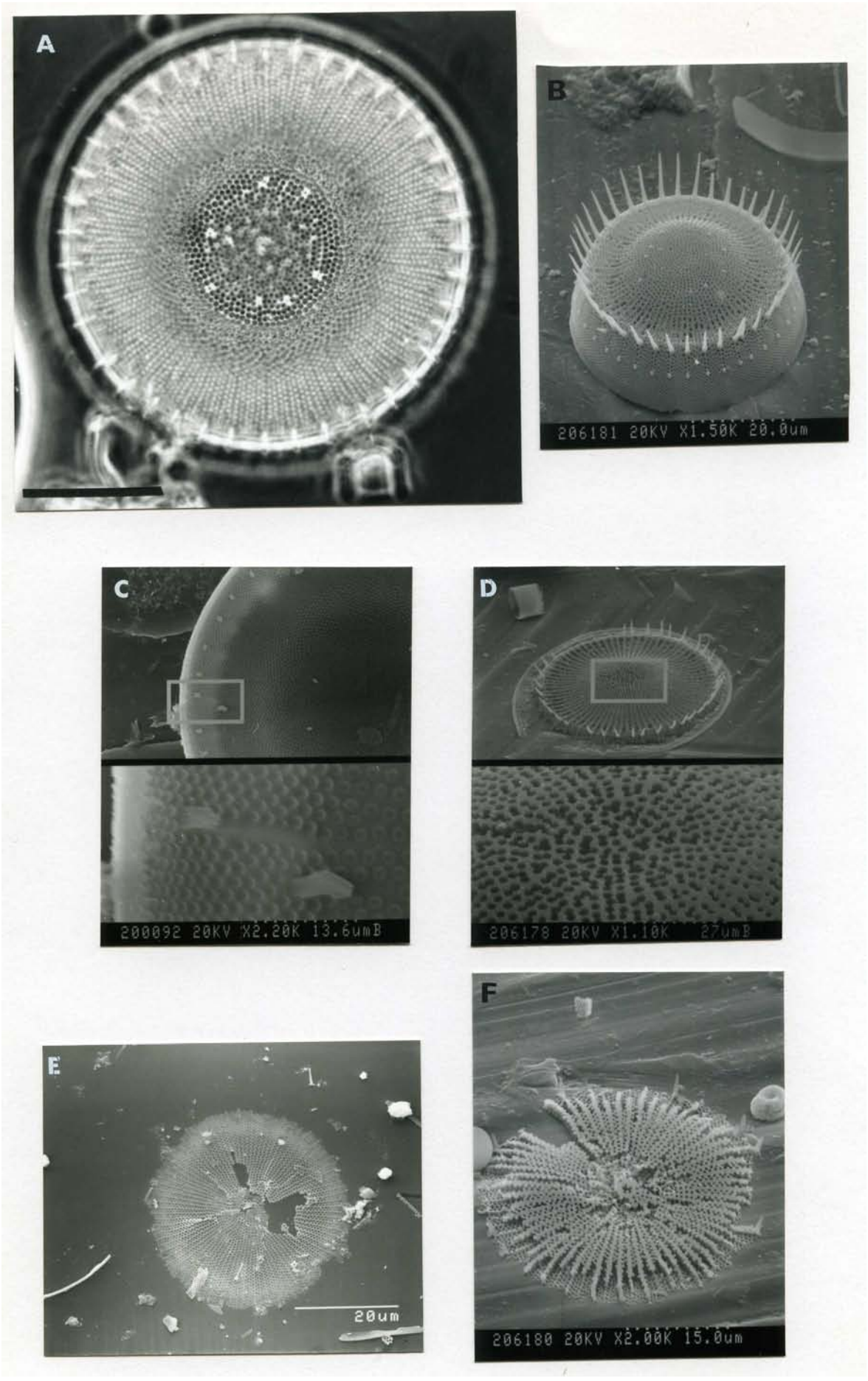

Figure A21. *Surirella ovalis*. a. Dissolution stage 1 (LM) – focus A. Scale bar = 20 µm. b. Dissolution stage 1 (LM) – same valve as (a), focus B. Scale bar = 20 µm. c. Dissolution stage 1 (SEM), valve view. d. Dissolution stage 1 (SEM), girdle view. e. Dissolution stage 2 (SEM), internal view. Note dissolution at valve edges. f. Dissolution stage 2 (SEM), external view; as (e). g. Dissolution stage 3 (SEM), internal view. Note loss of intercostal areas of valve, and distinct margin.

Figure A21 (Ryves et al.)

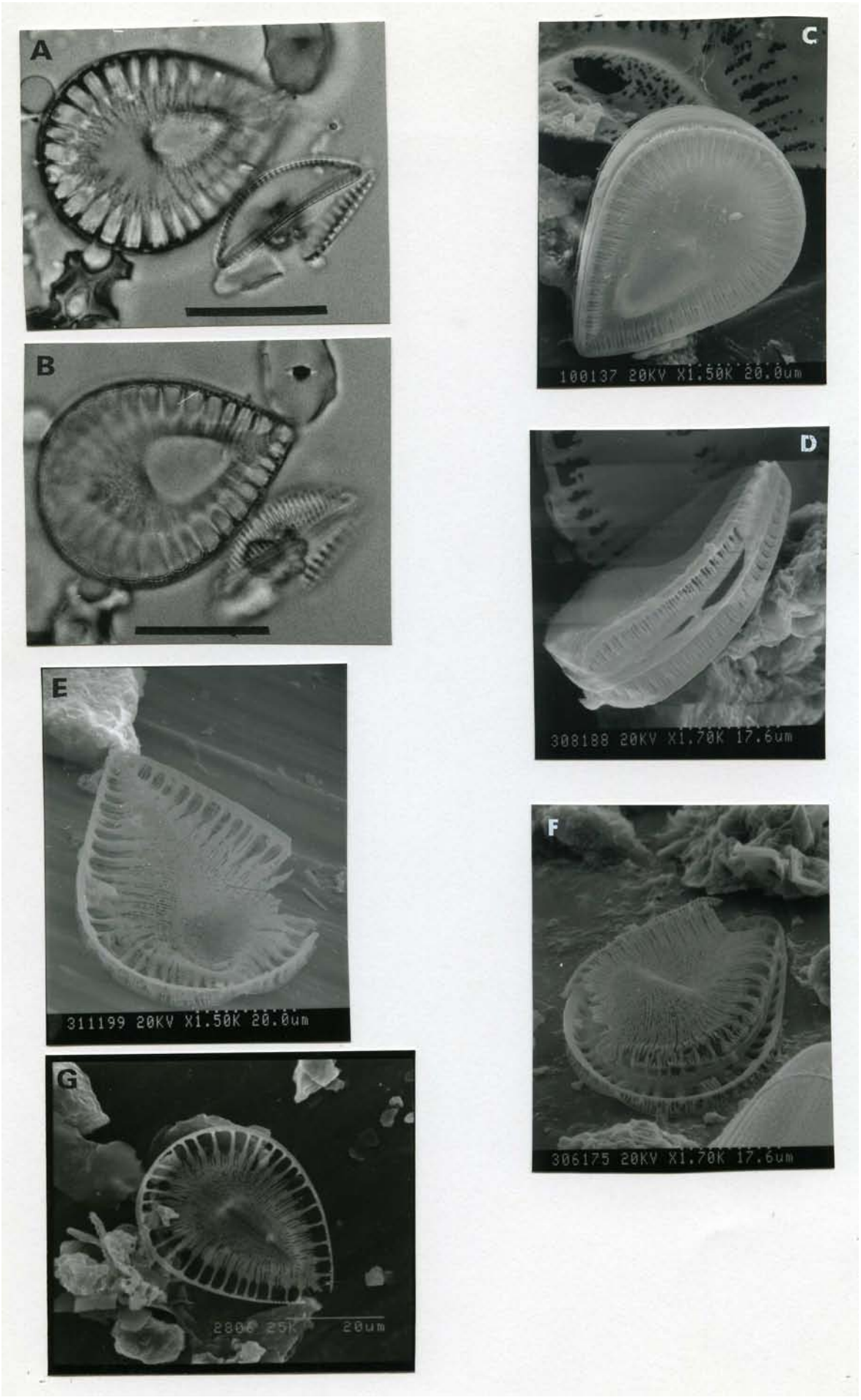

Figure A22. *Surirella striatula*. a. Dissolution stage 1 (LM). Scale bar = 30 µm. b. Dissolution stage 1 (LM). Scale bar = 25 µm. c. Dissolution stage 1 (SEM). d. Dissolution stage 2 (SEM), showing robust valve ribs and margin. e. Dissolution stage 2 (SEM), as (d). f. Dissolution stage 3 (SEM). Marginal rim is progressively dissolved.

Figure A22 (Ryves et al.)

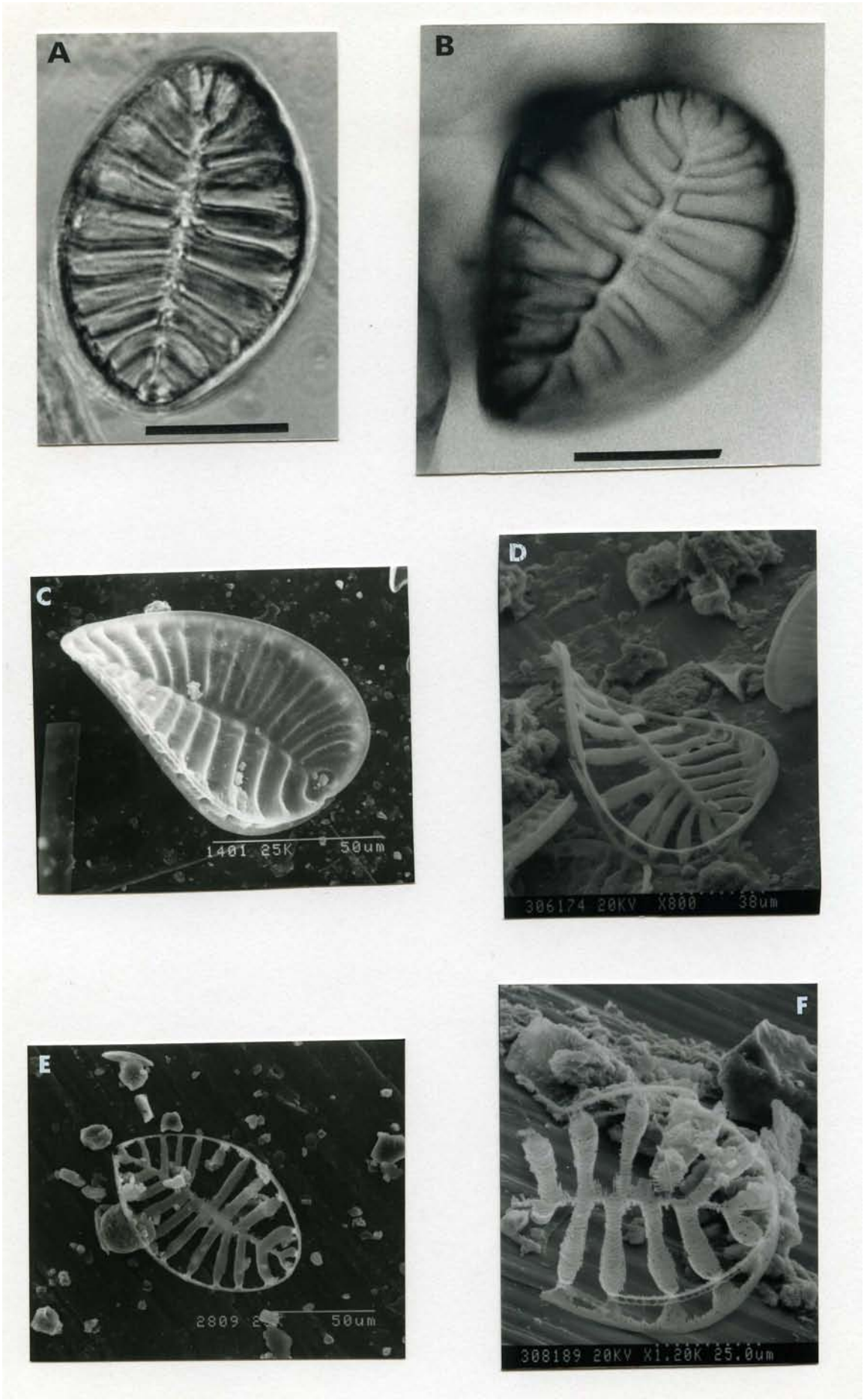

Figure A23. *Synedra fasciculata* (a–e) & *S. pulchella* (f, g). a. Dissolution stage 1 (SEM). b. Dissolution stage 2 (SEM) – see (d). c. Dissolution stage 1 (SEM). d. Dissolution stage 2 (SEM), detail of (b). Note dissolution of internal striae structure. e. Dissolution stage 2 (LM), as (d). Scale bar = 10 µm. f. Dissolution stage 1 (SEM). g. Dissolution stage 3 (SEM). The central inflation of this taxon is a distinct "dissolution taxon."

Figure A23 (Ryves et al.)